iScience

CellPress
OPEN ACCESS

Article

Sox9 mediates autophagy-dependent vascular smooth muscle cell phenotypic modulation and transplant arteriosclerosis

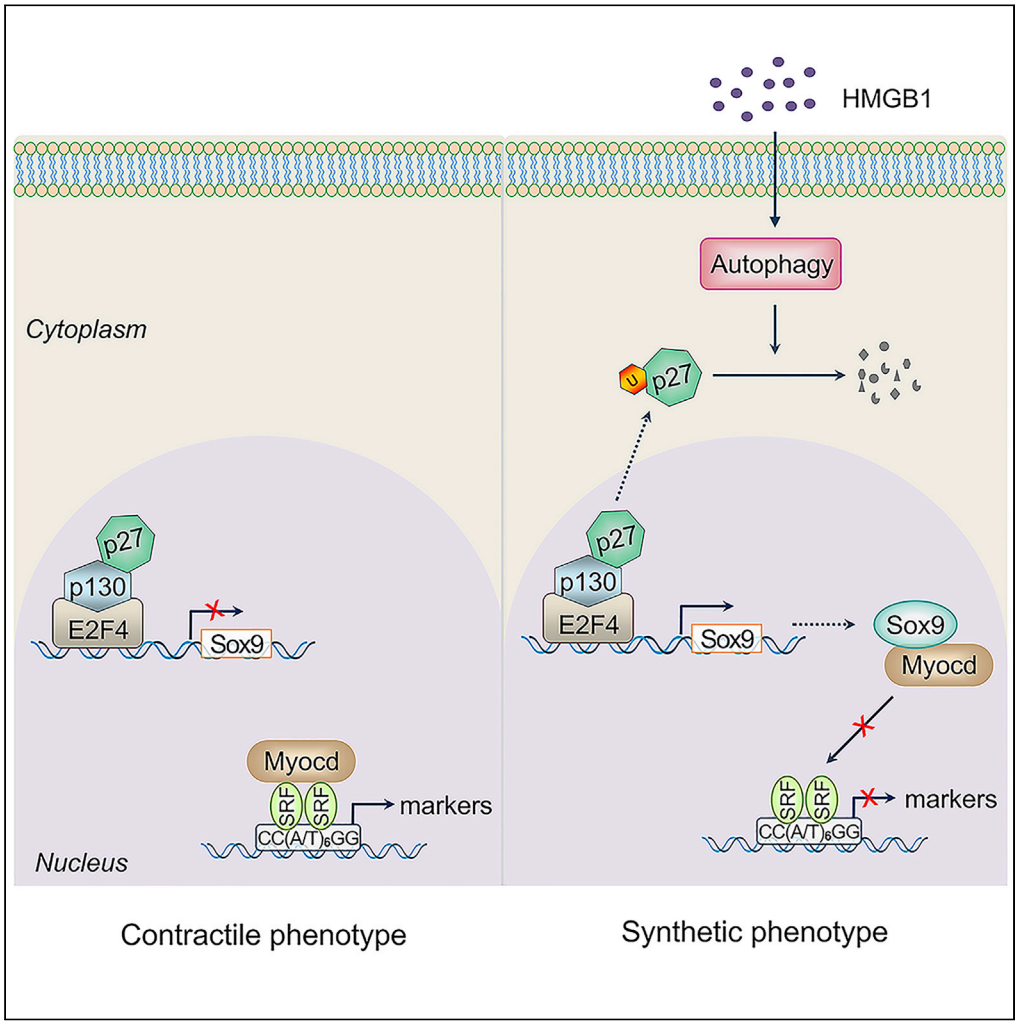

Qihong Yu, Jin-Xin Liu, Xichuan Zheng, ..., Chuanzheng Yin, Wei Li, Zifang Song

drwli@hust.edu.cn (W.L.)
zsong@hust.edu.cn (Z.S.)

Highlights

Sox9 expression in the media of aortic allografts promotes vSMC phenotypic modulation

Autophagy activation upregulates Sox9 expression by degrading p27 protein in vSMCs

p27 binds to p130/E2F4 complex on the Sox9 promoter and inhibits its expression

VSMC-specific Sox9 knockdown in aortic allografts delays transplant arteriosclerosis

Yu et al., iScience 25, 105161
October 21, 2022
https://doi.org/10.1016/j.isci.2022.105161

iScience

CellPress
OPEN ACCESS

Article

Sox9 mediates autophagy-dependent vascular smooth muscle cell phenotypic modulation and transplant arteriosclerosis

Qihong Yu,[1,2,6] Jin-Xin Liu,[5,6] Xichuan Zheng,[3] Xueke Yan,[3] Peng Zhao,[3] Chuanzheng Yin,[3] Wei Li,[4,*] and Zifang Song[3,7,*]

SUMMARY

Vascular smooth muscle cell (vSMC) phenotypic modulation is a dynamic pathogenesis process implicated in neointimal formation and transplant arteriosclerosis (TA). Transcription factor Sox9 functions to establish cell type and wound healing, but little is known about its transcriptional regulation in vSMCs and its roles in the development of TA. Here, we found an increased Sox9 expression in aortic allografts and in HMGB1-treated vSMCs *in vitro*, accompanied by the downregulation of vSMC markers. Notably, vSMC-specific *Sox9* knockdown in aortic allografts attenuated neointimal formation through preventing vSMC phenotypic modulation following transplantation. We further indicated that HMGB1 induced Sox9 expression and vSMC phenotypic modulation through activating autophagy to degrade $p27^{Kip1}$. Mechanistically, $p27^{Kip1}$ bound to the *Sox9* promoter in vSMCs together with p130/E2F4 complex, by which it restrained *Sox9* transcriptional expression. These findings uncover a fundamental role of Sox9 in mediating autophagy-dependent vSMC phenotypic modulation and TA, offering a therapeutic approach for vascular pathologies.

INTRODUCTION

Organ transplantation is a standard surgical treatment for many patients undergoing end-stage organ failure. Recent advances in immunosuppressive therapy have greatly improved short-term graft survival through declining the incidence of acute rejection episodes; however, the occurrence of chronic rejection seems inevitable and greatly challenges the long-term outcomes of the graft and patient survival (Chih et al., 2016; Lodhi et al., 2011). The pathological hallmark of chronic rejection of various organ transplants is transplant arteriosclerosis (TA), which features the diffuse and concentric intimal thickening arising from the accumulation of proliferating vascular smooth muscle cells (vSMCs) and deposition of extracellular matrix in graft arteries, enhancing the risk of progressive luminal narrowing and ultimately ischemic graft failure (Chih et al., 2016; Mitchell and Libby, 2007). Although the pathogenesis of TA is complex and incompletely understood, it is becoming clear that immunological damage to graft vasculature initiates a cascade of inflammatory events entering the injured grafts, which is followed by massive production of cytokines and growth factors, driving changes in vSMC behavior and widespread repair (Boersema et al., 2012; Mitchell and Libby, 2007; Owens et al., 2004). Because of the substantial phenotypical plasticity, vSMCs may lose their contractile, differentiated properties upon injury and transform into a synthetic, de-differentiated phenotype losing well-characterized vSMC marker genes, such as *α-smooth muscle actin* (*Acta2*), *Transgelin* (*Tagln*) and *Calponin1* (*Cnn1*), and subsequently migrating and proliferating (Owens et al., 2004). Studies in a rat model of aortic allografts demonstrate that phenotypic changes in vSMCs within graft vessels occur in aortic allografts as early as one week after transplantation (Bojakowski et al., 2000). We and others have established that synthetic vSMC proliferation and migration toward the intimal layer are closely related to the formation of neointimal lesions in allografts (Boersema et al., 2012; Bojakowski et al., 2000; Yu et al., 2018). Therefore, elucidating the molecular mechanisms governing vSMC phenotypic modulation may offer a novel therapeutic approach to the development of TA.

Sex-determining region Y box 9 (Sox9) is a member of the Sry-related Sox transcription factor family classified into different subgroups termed A to H, and has been initially described to determine cell fate throughout embryonic development (Gordon et al., 2009; Schepers et al., 2002). Sox9 belongs to the

[1]Hepatic Surgery Center, Tongji Hospital, Tongji Medical College, Huazhong University of Science and Technology, Wuhan 430030, China

[2]Clinical Medical Research Center of Hepatic Surgery at Hubei Province, Wuhan 430030, China

[3]Department of Hepatobiliary Surgery, Union Hospital, Tongji Medical College, Huazhong University of Science and Technology, Wuhan 430022, China

[4]Departments of Gerontology, Union Hospital, Tongji Medical College, Huazhong University of Science and Technology, Wuhan 430022, China

[5]Department of Otolaryngology-Head and Neck Surgery, Tongji Hospital, Tongji Medical College, Huazhong University of Science and Technology, Wuhan 430030, China

[6]These authors contributed equally

[7]Lead contact

*Correspondence: drwli@hust.edu.cn (W.L.), zsong@hust.edu.cn (Z.S.)

https://doi.org/10.1016/j.isci.2022.105161

SoxE subgroup and is composed of four functional domains, a dimerization domain, a DNA-binding HMG domain, and two C-terminal transactivation domains that enable Sox9 to possess versatile functions implicated in cell differentiation, proliferation and reprogramming depending on distinct cellular contexts (Jo et al., 2014; Schepers et al., 2002). Current studies have also characterized its involvement in several acquired diseases. A causal role for Sox9 in producing a continuous supply of cells from stem and progenitor cells that maintain self-renewal and regeneration under homeostasis and upon injury is emerging (Furuyama et al., 2011). In addition to that in the stem cell-based repair models, Sox9 expression in injured kidneys has been positively linked to tubular epithelial cell proliferation and the regeneration of functional tubular epithelium (Kumar et al., 2015), supporting the idea of an alternative repair process for Sox9 designed to rapidly confer any surviving mature cell with transient reparative potential. Generally, Sox9 controls targeted gene transcription and displays biological functions by acting in concert with its partner proteins. The binding of HMG to a minor groove of DNA double helix enables DNA bending, which allows the Sox9-partner complex to selectively bind to nonadjacent transcription starting sites of target genes, which subsequently initiates a series of transcriptional events (Hou et al., 2017). For instance, Sox9 can bind to and activate the enhancer region of cartilage-specific markers together with the Sox5/Sox6 complex that highlights the classical function of Sox9 in chondrocyte differentiation (Akiyama et al., 2002). Moreover, the association of Sox9 with myocardin (Myocd) may restrain its binding to the serum response factor (Srf)-CC(A/T)6GG (CArG) complex located in the promoter region of several vSMC marker genes, resulting in the loss of these genes and vSMC dedifferentiation (Owens et al., 2004; Xu et al., 2012). Support for this notion comes from studies on the function of Sox9 in atherosclerosis (Naik et al., 2012) and aneurysm (Orriols et al., 2016) showing that increased Sox9 expression is associated with the osteochondrogenic transition of vSMCs and vascular calcification. To date, although the importance of Sox9 in diverse disease states has been uncovered, certain aspects of Sox9 function and regulation in the context of TA remain unclarified.

Here, using a well-established aortic interposition allograft model, we specifically show potent restriction of *Sox9* knockdown to vSMC phenotypic modulation and proliferation, which is associated with impaired neointimal lesion formation and lumen stenosis in aortic allografts. *In vitro* studies indicate that autophagy activation is closely related to the transcriptional expression of *Sox9* and vSMC phenotypic modulation because it promotes $p27^{Kip1}$ (p27) protein ubiquitination and subsequent degradation. Furthermore, we identify that p27 can directly bind to *Sox9* promoter and restrain *Sox9* transcription by associating with the retinoblastoma transcriptional corepressor like 2 (Rbl2/p130)/E2F transcription factor 4 (E2F4) transcription complex that directly targets *Sox9*. Our studies describe a potential mechanistic basis for the development of TA and shed light on a promising therapeutic strategy for chronic allograft failure via targeting Sox9.

RESULTS

Upregulated expression of Sox9 in medial vSMCs of aortic allografts and HMGB1-treated vSMCs

To dissect the transcriptomic changes in vSMCs in the aortic grafts upon aortic transplantation, we initially employed rat graft arteriosclerosis models and 2 weeks later extracted total RNA from medial vSMCs isolated from aortic grafts. The non-transplanted abdominal aorta from Brown Norway (BN) and Lewis rats were used to exclude the influence of genetic background. RNA sequencing analysis showed extensive differentially expressed genes in aortic allogartfs (BN-Lewis) compared with those in isograft (Lewis-Lewis) controls, with 3493 up-regulated and 2574 down-regulated genes ($|\log2 \text{ (fold change)}| > 1$; p adj. < 0.01). In isografts, gene expression profile in the media was similar to that in non-transplanted aortas (Figure 1A). Gene ontology (GO) analysis of these differentially expressed genes revealed the enrichment in several processes related to immune/inflammatory response, and cell functions including positive regulation of cell proliferation, negative regulation of cell differentiation, cytoskeleton organization and extracellular matrix organization (Figure 1B), which are associated with vSMC phenotypic modulation (Owens et al., 2004). Venn diagram analysis identified up-regulated *Sox9* and downed-regulated *integrin subunit beta 1* (*Itgb1*) commonly associated with these GO terms (Figure 1C), implying a possible correlation of these genes to vSMCs phenotypic modulation. Among these genes, transcription factor *Sox9* was selected for further study, and its increased expression in the medial cells of aortic allografts was confirmed by quantitative real-time PCR (qRT-PCR) (Figure 1D). Consistently, immunofluorescence staining of vascular sections exhibited extensive Sox9 signals in the medial layer of the aortic allografts and mirror allografts (Lewis-BN) at 2 weeks compared with that in corresponding isografts, notably with medial Acta2-positive

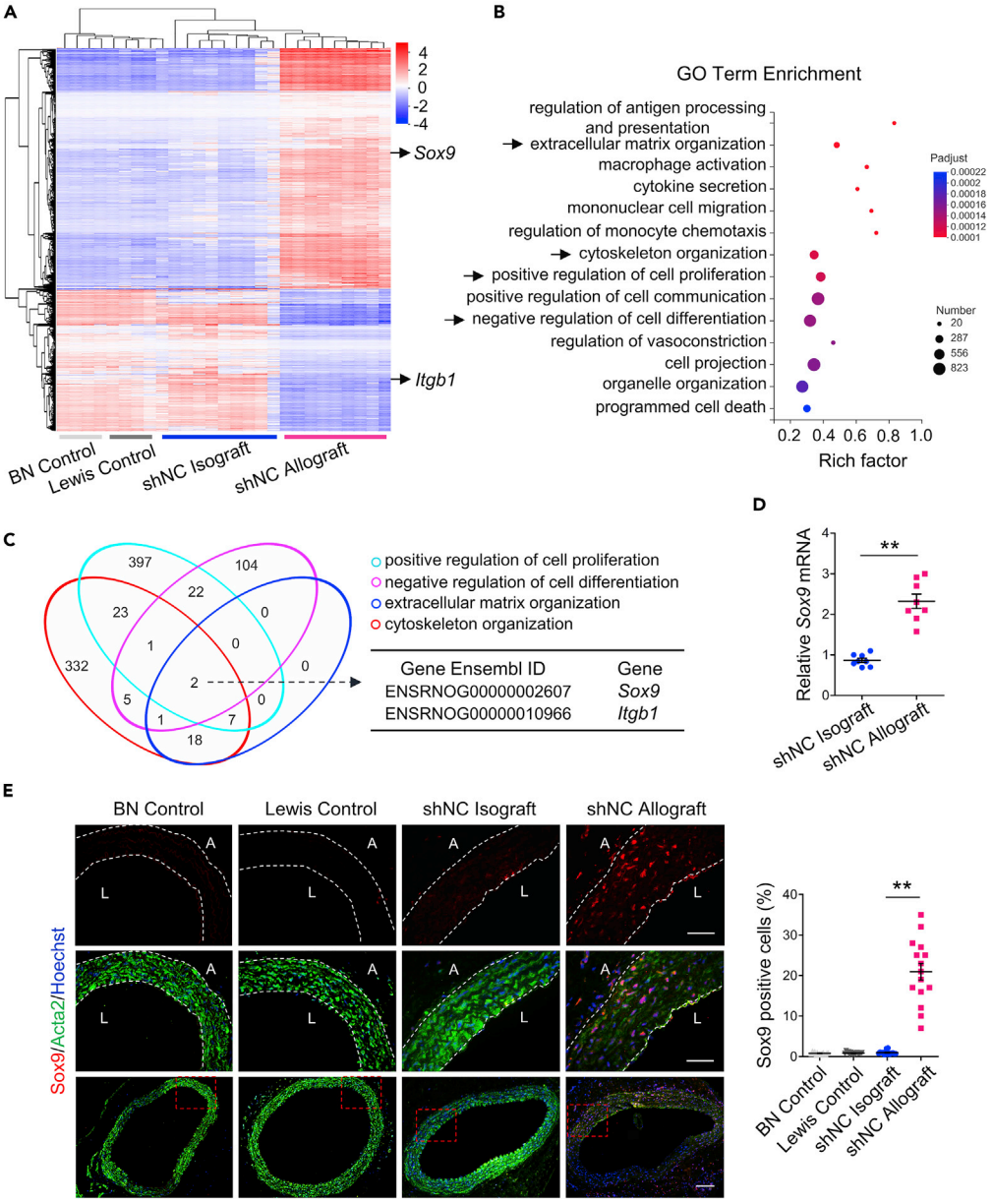

Figure 1. Upregulated expression of Sox9 in medial vSMCs of aortic allografts and HMGB1-treated vSMCs

(A) Heatmap shows differentially regulated genes (|log2FC(allograft/isograft)| > 1; *p* adjust <0.01) in the medial cells of non-transplanted aorta from Lewis (n = 4) and BN (n = 4) rats, isografts (Lewis-Lewis. n = 10 rats) and allografts (BN-Lewis. n = 9 rats) transfected with lentiviruses expressing negative control shRNA with a specific tagln promoter (shNC) 2 weeks after transplantation, as detected by preforming RNA sequencing.

(B) GO enrichment analysis shows selected GO terms of biological process of differentially regulated genes (DEGs). Size of circles represents the number of DEGs. *p* adjust values are displayed.

(C) Venn diagram shows the overlap between genes in indicated GO terms.

(D) qRT-PCR analysis of *Sox9* mRNA expression within medial cells of shNC isografts and shNC allografts 2 weeks after transplantation (means ± SEM **p < 0.01. n = 8 rats per group).

(E) Representative cross sections of aortic grafts coimmunostained for Sox9 (red) and Acta2 (green) 2 weeks after transplantation. Cell nuclei were stained with hoechst (blue). White dotted line outlines the media of the vascular wall. A, adventitial; L, lumen. Scale bar: 100 μm. Quantification of Sox9 positive cells in the media of aortic grafts (means ± SEM **p < 0.01. n = 15 rats per group).

vSMC colocalization (Figures 1E and S1), suggesting an increase in Sox9 expression in vSMCs in aortic allografts following transplantation.

High-mobility group box 1 (HMGB1) is one of the main pathogenic cytokines produced and secreted at the site of alloimmune injury, which contributes to transplant arteriosclerosis and chronic allograft dysfunction (Zou et al., 2021). Accordingly, enhanced mRNA expression of *Hmgb1* was detected in aortic allografts 2 weeks following transplantation compared with those in isograft controls (Figure S2A). Immunohistochemical staining confirmed increased Hmgb1 immunoreactivity in aortic allografts at 2 weeks accompanied by an increase in the nuclear and cytoplasmic distribution of Hmgb1 (Figure S2B). Moreover, in accordance with Hmgb1 production in aortic allografts, we noted that rats with aortic allografts had an increase in Hmgb1 serum levels from day 3 through day 7 and 14 after transplantation compared with those in isograft controls, as measured by ELISA (Figure S2C). Subsequently, we quantified the expression of Sox9 in primary cultured vSMCs in response to exogenous administration of recombinant HMGB1. In line with the findings *in vivo*, HMGB1 exposure elevated Sox9 expression compared with that in control cells (Figure S3A). Notably, the increase in Sox9 was mainly in the nucleus, as measured by immunofluorescence staining (Figure S3B), indicating that alloimmune injury and HMGB1 have a significant impact on Sox9 expression.

Sox9 drives the phenotypic modulation of vSMCs following transplantation

Given the results acquired from transcriptome analysis of aortic grafts, we further interrogated the relevance of Sox9 in phenotypic modulation of vSMCs. RNA sequencing analysis identified that vSMC marker genes (eg, *Cnn1*, *Acta2*, *Tagln*) expression in non-transplanted aortas from BN and Lewis rats were similar to that in aortic isografts, however, these genes were downregulated in aortic allografts at 2 weeks after transplantation (Figures S4A and S4B). The repression of these genes was further validated by qRT-PCR (Figure 2A) and immunofluorescence staining (Figure 2B), indicating vSMC phenotypic transition toward the dedifferentiated phenotype. In addition, to gain insight into the regulation of vSMC-derived Sox9 in the phenotypic modulation of vSMCs and neointimal formation, we established a rat model of aortic transplantation with stable knockdown of *Sox9* in medial vSMCs in aortic allografts using a lentivirus-mediated transfer of shRNA targeting *Sox9* gene (sh*Sox9*) driven by the smooth muscle-specific *Tagln* promoter. Significant knockdown of *Sox9* mRNA was observed in aortic allografts at 2 weeks. Of relevance, selective knockdown of *Sox9* in medial vSMCs drastically mitigated the alloimmune injury-triggered inhibition of mRNA expression and immunoreactivity of *Cnn1*, *Acta2* and *Tagln* 2 weeks after transplantation (Figures 2A and 2B), suggesting a crucial role for Sox9 in controlling vSMC phenotypic modulation. In line with these observations *in vivo*, both the expression of *Cnn1*, *Acta2* and *Tagln* were declined in vSMCs exposed to HMGB1 stimulation, whereas the reduction in these genes were largely ameliorated in *Sox9*-knockdown vSMCs. Notably, *Sox9* silencing in vSMCs, even with HMGB1 stimulation, failed to directly alter myocardin (Myocd) or Srf expression (Figures 2C and 2D). Collectively, these data suggest that Sox9 controls vSMC phenotypic modulation in response to alloimmune injury and HMGB1 stimulation.

Sox9 facilitates vSMC proliferation, migration and transplant arteriosclerosis in rat aortic allografts

Phenotypic modulation of vSMCs nearly always precedes cell migration and proliferation into the intimal layer of the artery, which contributes critically to vascular repair and neointimal formation after vascular injury (Owens et al., 2004). Immunohistochemical staining verified the increased amounts of PCNA-positive cells in the media of aortic allografts relative to the isograft group 2 weeks after transplantation, whereas selective knockdown of *Sox9* abolished this effect in aortic allografts, indicating the positive involvement of Sox9 in vSMC proliferation (Figure 3A). *In vitro*, we found that HMGB1-treated vSMCs exhibited greater proliferative activity compared with shRNA control vSMCs, whereas these effects were abolished in *Sox9*-knockdown vSMCs (Figures 3B and 3C). Moreover, knockdown of *Sox9* in vSMCs markedly reduced the number of migrated cells in response to HMGB1 treatment as measured by Transwell assay (Figure 3D), indicating that Sox9 promotes the proliferative and migratory processes of dedifferentiated vSMCs.

Considering the functional contribution of Sox9 to vSMC phenotypic modulation in aortic allografts and results of *in vitro* vSMC functional studies, we hypothesized that vSMC-derived Sox9 may control the development of transplant arteriosclerosis. Aortic grafts were isolated from recipient rats 8 weeks after undergoing aortic transplantation, and subsequently histological and immunofluorescence staining analyses were performed. Compared with isograft controls, aortic allografts showed a substantial increase in

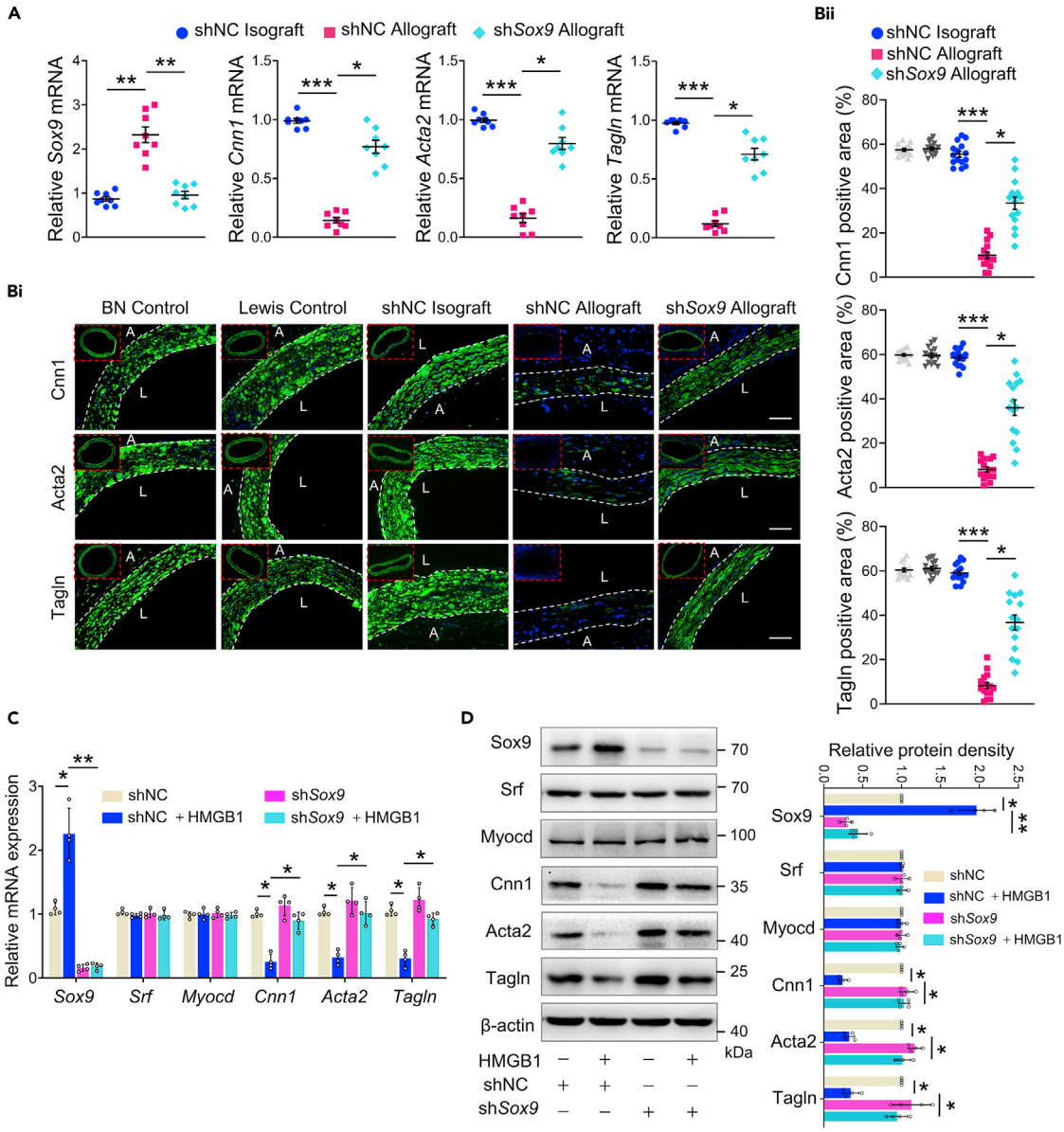

Figure 2. Sox9 drives the phenotypic modulation of vSMC following transplantation

(A) qRT-PCR analysis of *Sox9*, *Cnn1*, *Acta2* and *Tagln* mRNA expression within the media of aortic isografts and allograft transfected with sh*Sox9* or shNC 2 weeks after transplantation (means ± SEM *p < 0.05, **p < 0.01, ***p < 0.001. n = 8 rats per group).

(B) Representative cross sections of non-transplanted aorta, and sh*Sox9*-or shNC-transfected aortic grafts immunostained for Cnn1 (green), Acta2 (green) and Tagln (green) 2 weeks after transplantation (Bi). Cell nuclei were stained with hoechst (blue). Red boxes indicate the total sections. White dotted line outlines the media of the vascular wall. A, adventitial; L, lumen. Scale bar: 100 μm. Quantification of Cnn1, Acta2 and Tagln positive area in the media of aortic grafts (Bii) (means ± SEM *p < 0.05, ***p < 0.001. n = 15 rats per group).

(C and D) qRT-PCR and western blotting analyses of *Myocd*, *Srf*, *Sox9*, *Cnn1*, *Acta2* and *Tagln* expression in cultured vSMCs transfected with lentiviruses carring *Sox9*-targeting shRNA (sh*Sox9*) with a specific *Tagln* promoter or negative control shRNA (shNC) followed by HMGB1 (100 ng/mL) stimulation or not (means ± SEM *p < 0.05, **p < 0.01. n = 4).

neointimal lesions as measured by H&E and EVG staining, and these lesions were composed mainly of Acta2-positive cells (Figure 3E), indicating that the accelerated neointimal formation induced by alloimmune injury may be the result of excessive accumulation of proliferating vSMCs. Furthermore, we noted increased expression of Sox9 in the neointimal lesion of aortic allografts, and lentivirus-mediated knockdown of *Sox9* in vSMCs within aortic allografts lasted for 8 weeks (Figures S5A and S5B). Importantly, alloimmune injury-induced accumulation of vSMCs into neointimal lesions was greatly reduced in aortic

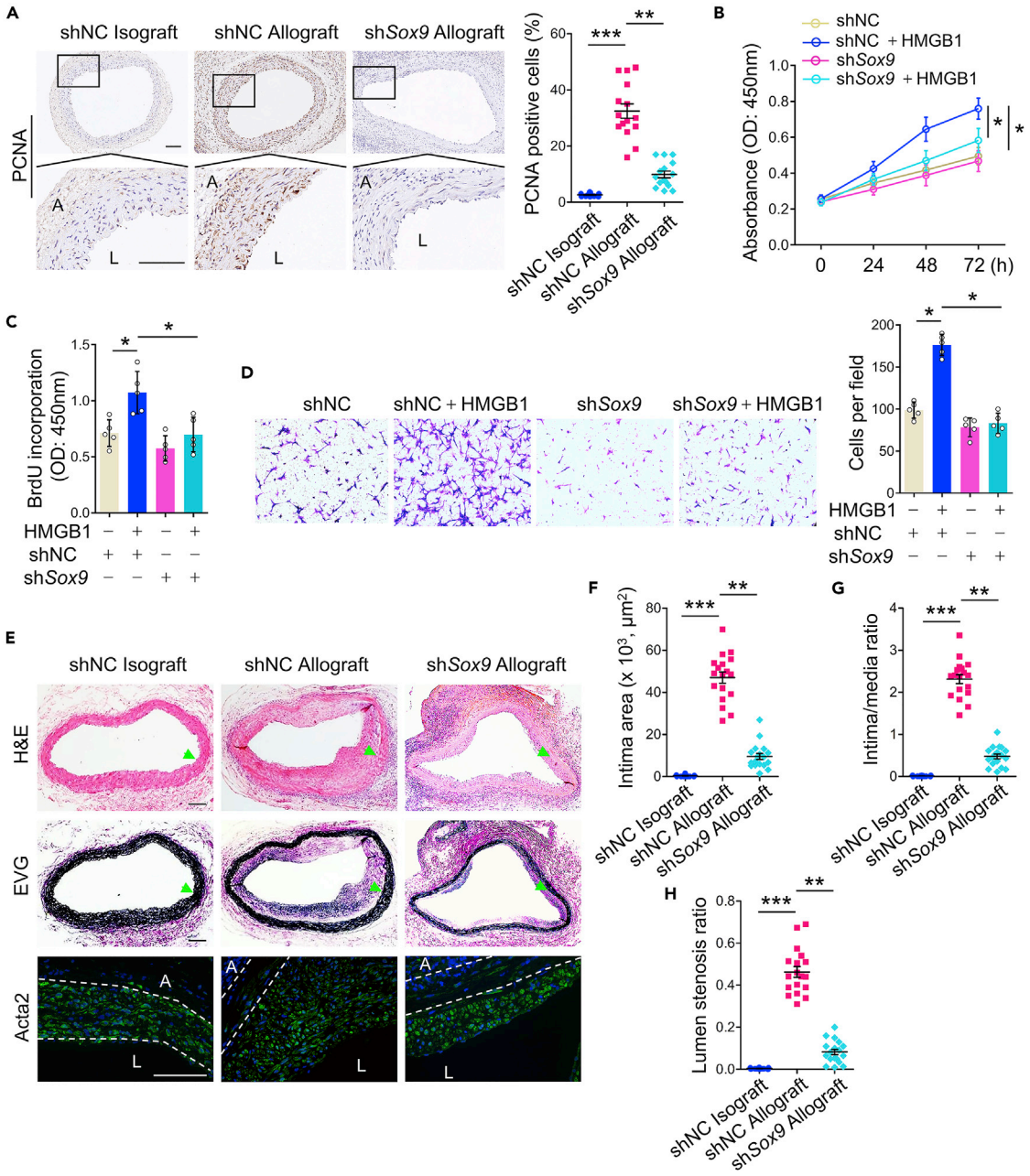

Figure 3. Sox9 facilitates vSMC proliferation, migration and transplant arteriosclerosis in rat aortic allografts

(A) Representative cross sections of shNC- or sh*Sox9*-transfected isografts and allografts immunostained for PCNA 2 weeks after transplantation. A, adventitial; L, lumen. Scale bar: 100 μm. Quantification of PCNA-positive cells in the media of aortic grafts (means ± SEM **p < 0.01, ***p < 0.001. n = 15 rats per group).

(B and C) vSMCs transfected with sh*Sox9* or negative control shNC were stimulated with or without HMGB1 (100 ng/mL), cell proliferation was evaluated by CCK-8 and BrdU incorporation assays as the measured absorbance at 450 nm (means ± SEM *p < 0.05. n = 5).

(D) Representative images of migrated vSMCs on the bottom of transwell membrane as detected by Transwell assays (means ± SEM *p < 0.05. n = 5).

(E) Representative images to show H&E staining, EVG staining and immunofluorescence staining of vSMC marker Acta2 in cross sections of aortic isografts and allografts transfected with shNC or sh*Sox9* 8 weeks after aortic transplantation. Green arrows denote the internal elastic lamina. White dotted line outlines the media of the vascular wall. A, adventitial; L, lumen. Scale bar: 100 μm.

(F–H) Quantification of of intimal area, intima/media ratio and lumen stenosis ratio (means ± SEM **p < 0.01, ***p < 0.001. n = 18 rats per group).

allografts with *Sox9* knockdown, leading to less neointimal formation (Figure 3E), as reflected by both a reduction in intima area (Figure 3F) and the ratio of intima to media area (Figure 3G), thus causing a substantial decline in the lumen stenosis ratio (Figure 3H). Together, these results highlight that vSMC-derived Sox9 contributes to the development of transplant arteriosclerosis by promoting vSMC accumulation in aortic allografts.

Autophagy is associated with increased Sox9 expression in vSMCs

Sox9 has been reported to be controlled at the transcriptional level or by the polyubiquitylation-degradation pathway (Luanpitpong et al., 2016; Sugiyama et al., 2017). Autophagy, as a crucial degradation process maintaining cellular homeostasis under stress conditions, has been associated with the regulation of vSMC function and the development of neointimal lesions (Lv et al., 2020). We considered the possibility that autophagy is involved in the phenotypic modulation of vSMCs as mediated by Sox9. As shown in Figure 4A, cross-sections of aortic allografts showed increased autophagy activation characterized by higher levels of autophagy-related protein LC3I/II signaling in the media of aortic allografts 2 weeks after transplantation versus the isograft control, while the change was associated with reduced Acta2-positive cells aortic allografts. Subsequently, performing transmission electron microscopy, we detected an increased number of double-membrane autophagosome and single-membrane autophagolysosome containing cargo in aortic allografts at 2 weeks, which highlights the increased autophagy flux in response to alloimmune injury (Figure 4B). We also deciphered the impact of HMGB1 treatment on autophagy activation in cultured vSMCs. In accordance with previous findings (Huebener et al., 2014), incubation of vSMCs with HMGB1 resulted in higher levels of the autophagy-related gene Atg5 expression and facilitated the formation of LC3II aggregates in concurrence with a significant reduction in the level of p62/SQSTM1 (p62) protein (Figure S6A), which acted as an adaptor protein of autophagy, with its decrease supporting increased autophagy activation (Rogov et al., 2014). Moreover, increased LC3I/II puncta formation and autophagosome/autophagolysosome structures were detected in the cytoplasm of vSMCs exposed to HMGB1 (Figure 4C), emphasizing a positive role for HMGB1 in autophagy activation.

Next, we screened the functional effect of autophagy on Sox9 expression. As shown in Figures 4D and 4E, genetic inhibition of autophagy via the transfection of *Atg5* siRNA significantly suppressed LC3II expression but promoted p62 protein levels, concurrent with a marked decrease in Sox9 expression even in the presence of HMGB1 treatment. Moreover, the addition of bafilomycin A1, which is an inhibitor of late-stage autophagy that could block the fusion of autophagosomes and lysosomes, facilitated the accumulation of LC3II and p62 proteins and exerted the same effect as *Atg5* knockdown on *Sox9* mRNA and protein expression (Figures 4F and 4G), highlighting a potential contribution of autophagy activation to *Sox9* transcriptional expression, which relies on the autophagy-lysosomal pathway. We then sought to determine whether autophagy affects the cellular localization of Sox9. Since increased Sox9 expression induced by HMGB1 was mainly located in the nucleus, *Atg5* knockdown or pharmacological inhibition of autophagy markedly inhibited Sox9 protein level in the nucleus; no significant change in the nuclear translocation of Sox9 was detected by immunofluorescence staining (Figure S6B) and western blotting (Figures S6C and S6D), and therefore, this mechanism subsequently eliminated from the mechanistic analysis.

Autophagy promotes vSMC phentopic modulation by upregulating Sox9

Exploring the effect of autophagy on vSMC phenotypic modulation, we found that *Atg5* knockdown significantly abrogated HMGB1-induced downregulation of *Cnn1*, *Acta2* and *Tagln* (Figures 5A and 5B). Blockade of lysosomal degradation pathway realized by bafilomycin A1 had the same effect as *Atg5* knockdown on these gene expression in the presence of HMGB1 stimulation (Figures 5C and 5D), suggesting that autophagy promotes vSMC phenotypic modulation, at least in part, by downregulating the transcriptional levels of vSMC marker genes. Considering the above findings regarding the functional contribution of autophagy to Sox9 expression, we then study the relevance of Sox9 in autophagy-regulated phenotypic modulation of vSMCs. As shown in Figures 5E and 5F, vSMCs with *Sox9* ectopic expression showed a marked downregulation of *Cnn1*, *Acta2* and *Tagln*. We further analyzed these genes expression in vSMCs cotransfected with *Atg5* siRNA and *Sox9* overexpressing plasmids upon HMGB1 stimulation, and found that ectopic expression of *Sox9* was able to restore HMGB1-triggered downregulation of vSMC marker genes in *Atg5*-knockdown vSMCs (Figure 5G), demonstrating that autophagy promotes vSMC phenotypic modulation by directly targeting Sox9. Furthermore, consistent with the suppression of *Sox9* knockdown in vSMC proliferative and migratory response, *Atg5* knockdown or pharmacological inhibitor also markedly

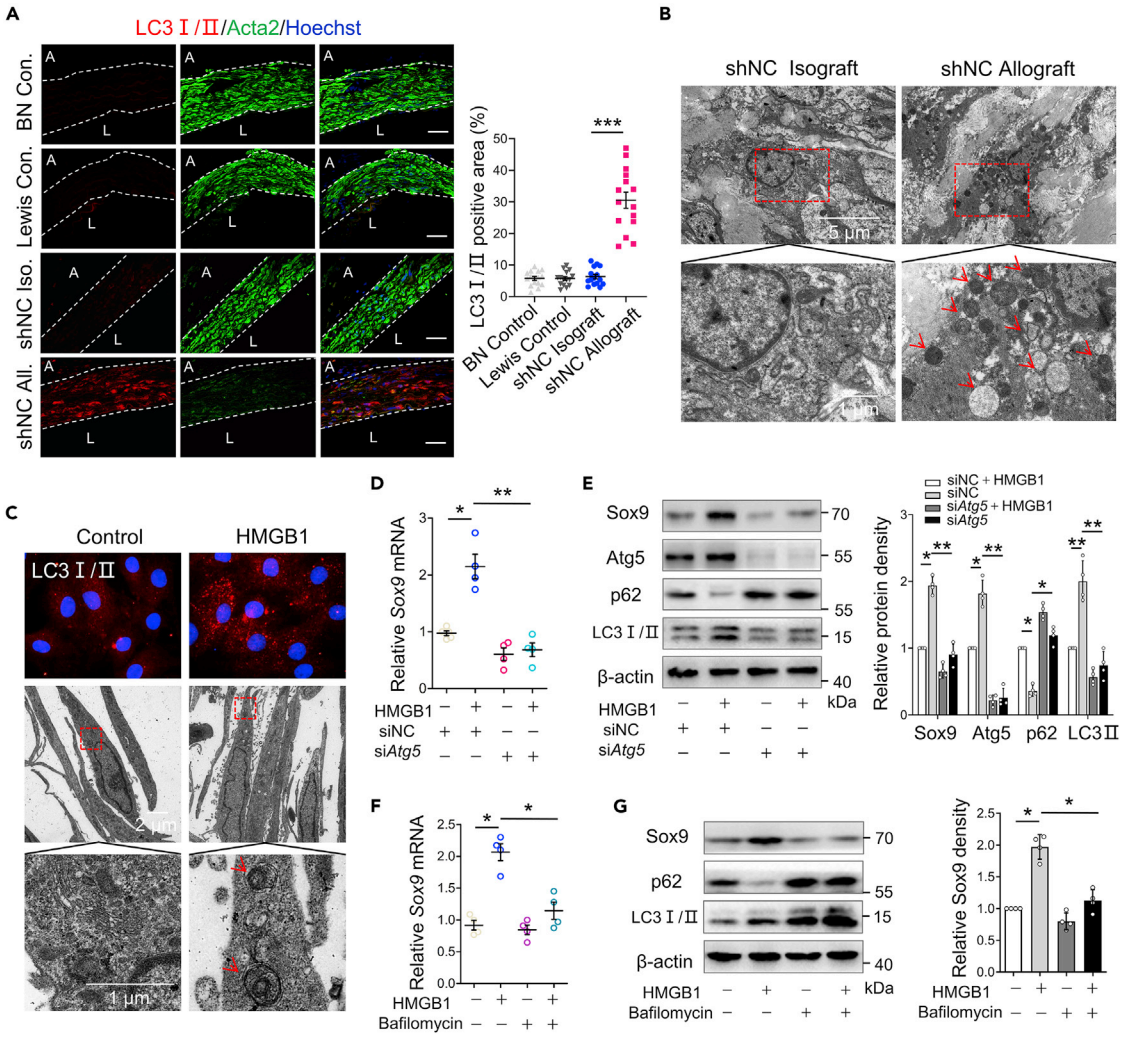

Figure 4. Autophagy is associated with increased Sox9 expression in vSMCs

(A) Representative cross sections of non-transplanted aorta and shNC-transfected aortic grafts coimmunostained for LC3I/II (red) and Acta2 (green) 2 weeks after transplantation. Cell nuclei were stained with hoechst (blue). White dotted line outlines the media of the vascular wall. A, adventitial; L, lumen. Scale bar: 100 μm. Quantification of LC3I/II-positive area in the media of aortic grafts (means ± SEM ***$p < 0.001$. n = 15 rats per group).

(B) Transmission electron microscopy images of double membrane autophagosome and single membrane autophagolysosome structures in aortic isografts and allografts transfected with shNC. Red boxes show the enlarged sections of aortic grafts.

(C) LC3I/II-stained fluorescent microscopy images of vSMCs treated with HMGB1 (100 ng/mL) for 48 h, transmission electron microscopy images of autophagosomes or autophagolysosomes in vSMCs stimulated with HMGB1 (100 ng/mL). Red boxes show the enlarged sections.

(D) vSMCs were transfected with small interfering RNA targeting *Atg5* (si*Atg5*) or its corresponding negative control (siNC) followed by HMGB1 (100 ng/mL) stimulation, *Sox9* mRNA expression was measured by qRT-PCR (means ± SEM *$p < 0.05$, **$p < 0.01$. n = 4).

(E) Western blotting analysis of Sox9, Atg5, p62 and LC3I/II expression in vSMCs transfected with si*Atg5* or siNC followed by HMGB1 (100 ng/mL) stimulation (means ± SEM *$p < 0.05$, **$p < 0.01$. n = 4).

(F and G) vSMCs pretreated with or without Bafilomycin A1 (200 nM) were stimulated with HMGB1. qRT-PCR analysis of *Sox9* mRNA expression. n = 4. Western blotting analysis of Sox9, p62 and LC3I/II protein expression (means ± SEM *$p < 0.05$. n = 4).

attenuated the proliferative (Figures 5H and 5I) and migratory (Figures 5J and 5K) capacities of vSMCs that enrich the mechanism that Sox9-mediated vSMC phenotypic modulation and neointimal formation in aortic allografts depends on the upstream autophagy activation.

Autophagy-mediated Sox9 expression relies on p27 degradation

We next investigated how autophagy in the cytoplasm enhanced the transcription of *Sox9* in the nucleus. Recently, p27 has been identified as a transcriptional corepressor that regulates different subsets of genes

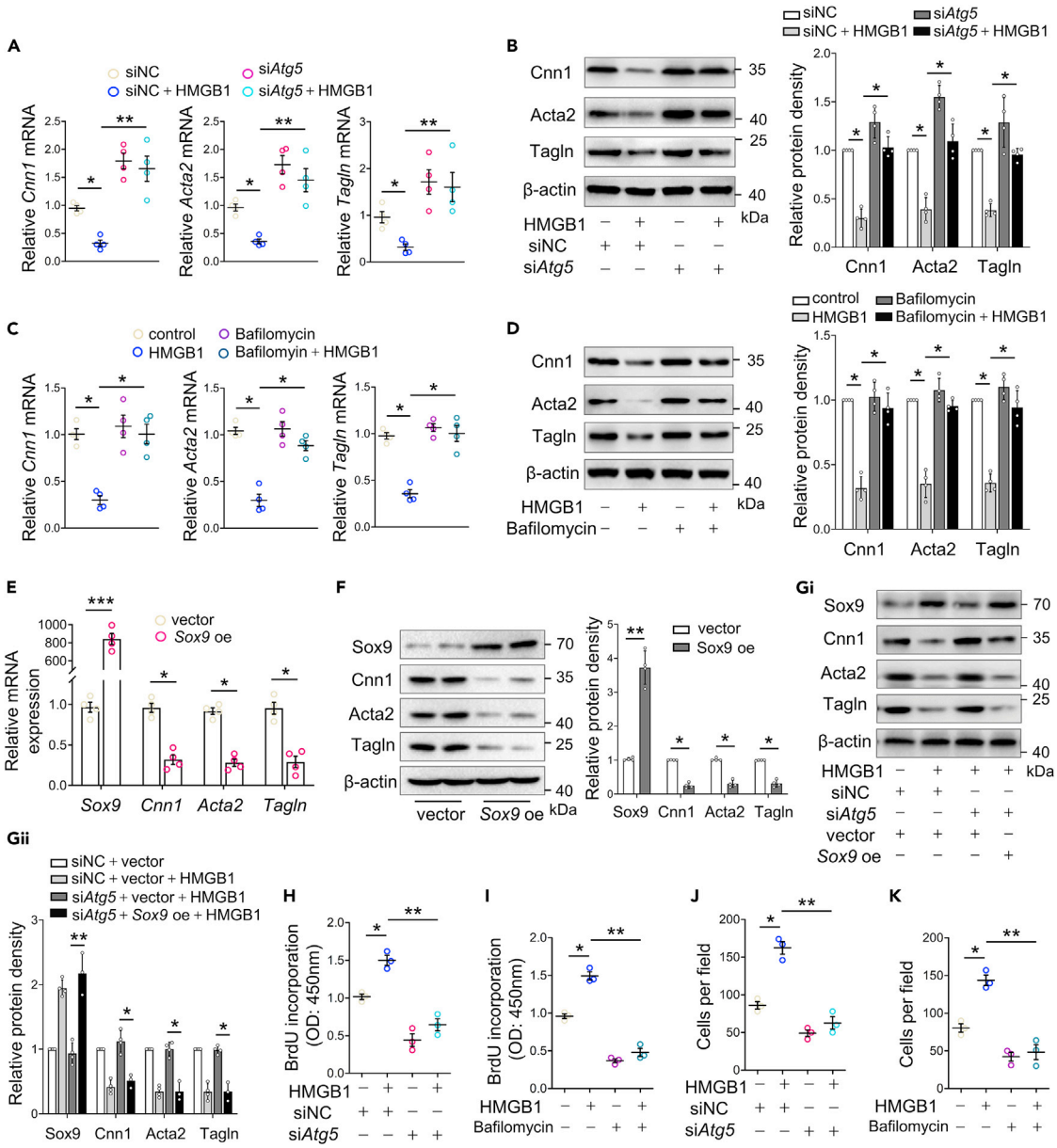

Figure 5. Autophagy promotes vSMC phentopic modulation by upregulating Sox9

(A and B) qRT-PCR and western blotting analyses of *Cnn1*, *Acta2* and *Tagln* mRNA and protein expression in vSMCs transfected with si*Atg5* or siNC followed by HMGB1 stimulation (means ± SEM *p < 0.05, **p < 0.01. n = 4).

(C and D) vSMCs pretreated with or without bafilomycin A1 were stimulated with HMGB1, mRNA and protein expression of *Cnn1*, *Acta2* and *Tagln* were measured by qRT-PCR and western blotting (means ± SEM *p < 0.05. n = 4).

(E and F) qRT-PCR and western blotting analyses of *Sox9*, *Cnn1*, *Acta2* and *Tagln* expression in vSMCs transfected with plasmids overexpressing *Sox9* (*Sox9* oe) or its control vector (vector) (means ± SEM *p < 0.05, **p < 0.01, ***p < 0.001. n = 4).

(G) vSMCs were cotransfected with *Atg5* siRNA and *Sox9* overexpressing plasmid together with HMGB1 (100 ng/mL) stimulation, protein expression of Sox9, Cnn1, Acta2 and Tagln were determined (means ± SEM *p < 0.05, **p < 0.01. n = 4). (H and I) BrdU incorporation assay was performed in si*Atg5*-transfected and Bafilomycin A1-pretreated vSMCs exposed to HMGB1 (means ± SEM *p < 0.05, **p < 0.01. n = 3).

(J and K) The migration ability of si*Atg5*-transfected and Bafilomycin A1-pretreated vSMCs exposed to HMGB1 was evaluated by Transwell assay (means ± SEM *p < 0.05, **p < 0.01. n = 3).

by binding to transcription factors (Pippa et al., 2012). We wondered whether p27 makes a functional contribution to Sox9 expression in vSMCs. Intriguingly, no statistical difference in *p27* mRNA level was observed in HMGB1-treated vSMCs at various timepoints (Figure 6A), while HMGB1 stimulation resulted in lower p27

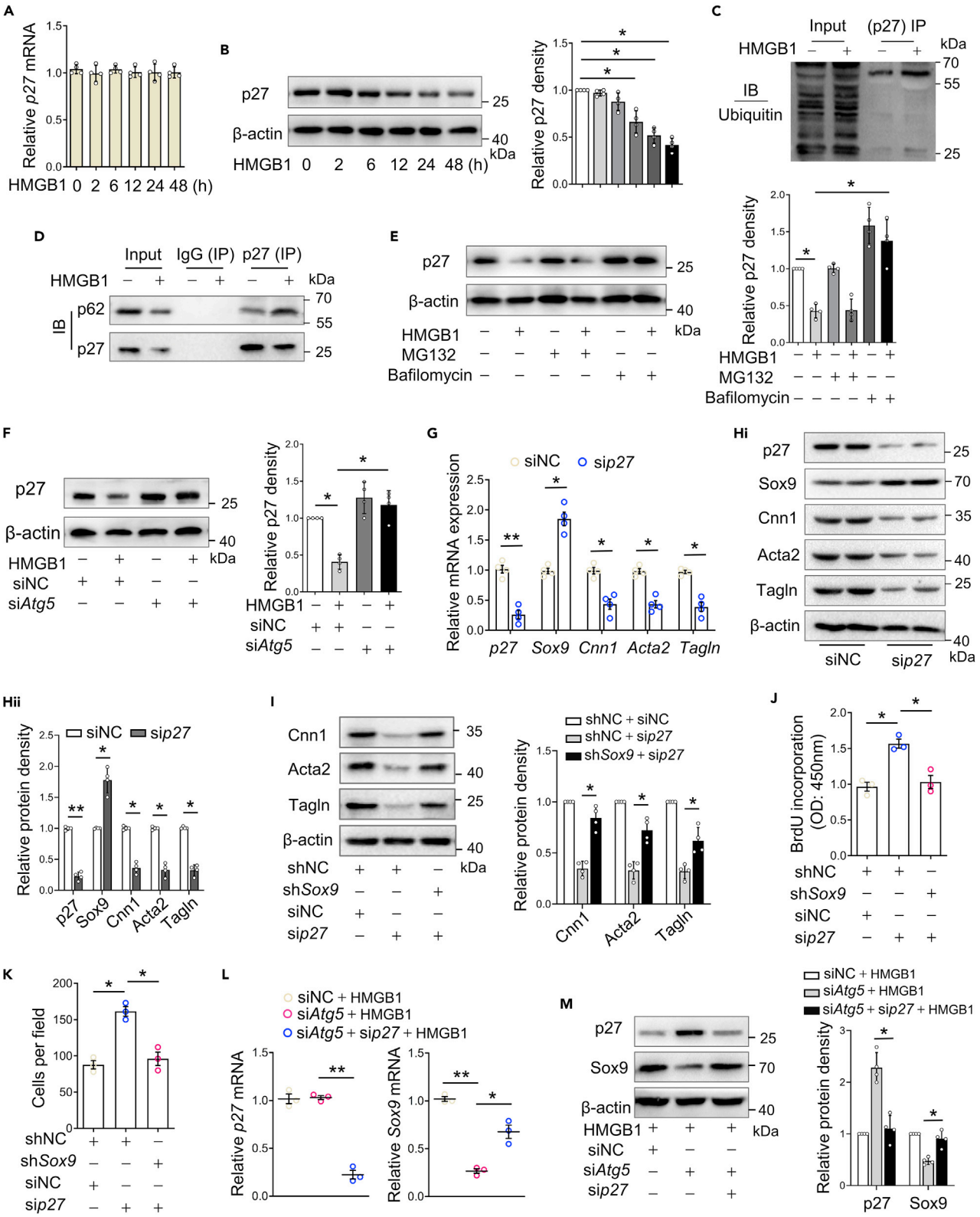
A
Relative p27 mRNA
HMGB1 0 2 6 12 24 48 (h)
B
p27
β-actin
HMGB1 0 2 6 12 24 48 (h)
kDa
Relative p27 density
C
Input
(p27) IP
HMGB1
IB
Ubiquitin
kDa
Relative p27 density
HMGB1
MG132
Bafilomycin
D
Input
IgG (IP)
p27 (IP)
HMGB1
IB
p62
p27
kDa
E
p27
β-actin
HMGB1
MG132
Bafilomycin
kDa
F
p27
β-actin
HMGB1
siNC
siAtg5
kDa
Relative p27 density
G
siNC
sip27
Relative mRNA expression
p27
Sox9
Cnn1
Acta2
Tagln
Hi
p27
Sox9
Cnn1
Acta2
Tagln
β-actin
siNC
sip27
kDa
Hii
siNC
sip27
Relative protein density
p27
Sox9
Cnn1
Acta2
Tagln
I
Cnn1
Acta2
Tagln
β-actin
shNC
shSox9
siNC
sip27
kDa
shNC + siNC
shNC + sip27
shSox9 + sip27
Relative protein density
Cnn1
Acta2
Tagln
J
BrdU incorporation (OD: 450nm)
shNC
shSox9
siNC
sip27
K
Cells per field
shNC
shSox9
siNC
sip27
L
siNC + HMGB1
siAtg5 + HMGB1
siAtg5 + sip27 + HMGB1
Relative p27 mRNA
Relative Sox9 mRNA
M
p27
Sox9
β-actin
HMGB1
siNC
siAtg5
sip27
kDa
siNC + HMGB1
siAtg5 + HMGB1
siAtg5 + sip27 + HMGB1
Relative protein density
p27
Sox9

Figure 6. Autophagy-mediated Sox9 expression relies on p27 degradation

(A and B) qRT-PCR and western blotting analyses of *p27*^{Kip1} (*p27*) expression in vSMCs exposed to HMGB1 (100 ng/mL) for indicated time (means ± SEM *p < 0.05. n = 4).

(C and D) vSMCs were stimulated with HMGB1 for 48 h, co-IP assay was performed to analyze the ubiquitination of p27 using anti-ubiquitin (n = 4); Binding of p27 and p62 was determined by immunoprecipitating p27 (n = 4).

(E) vSMCs pretreated with Bafilomycin A1 (200 nM) or MG132 (5 μM) were stimulated with or without HMGB1 (100 ng/mL) for 48 h, p27 protein level was determined by western blotting analysis, and densitometric analysis of blots was performed (means ± SEM *p < 0.05. n = 4).

(F) western blotting analysis and quantification of p27 expression in vSMCs transfected with si*Atg5* or siNC followed by HMGB1 stimulation (means ± SEM *p < 0.05. n = 4).

(G and H) qRT-PCR and western blotting analyses of *p27* expression in vSMCs transfected with si*p27* or siNC (means ± SEM *p < 0.05, **p < 0.01. n = 4).

(I and J) vSMCs were cotransfected with sh*Sox9* and si*p27*, Cnn1, Acta2 and Tagln expression were detected by western blotting (means ± SEM *p < 0.05. n = 4); Cell proliferation was evaluated by BrdU incorporation assay (means ± SEM *p < 0.05. n = 3); Cell migration was detected by Transwell assay (means ± SEM *p < 0.05. n = 3).

(L and M) vSMCs were cotransfected with si*Atg5* and si*p27* together with or without HMGB1, mRNA expression of *p27* and *Sox9* were detected by qRT-PCR (means ± SEM *p < 0.05, **p < 0.01. n = 3); p27 and Sox9 protein expression were measured by western blotting (means ± SEM *p < 0.05. n = 4).

protein expression versus that of the control cells (Figure 6B), revealing that HMGB1 may downregulate p27 protein expression by mediating its homeostatic levels. Support the idea comes from previous reports that p27 is degraded through the proteasomal or autophagic pathways (Jia et al., 2015; Zhao et al., 2019). co-IP assays indicated that anti-p27 antibody arrested two ubiquitinated proteins of approximately 62 and 27 kDa, molecular weights consistent with the p62 and p27 bands, respectively, and the ubiquitination levels of these proteins were increased in HMGB1-treated vSMCs (Figure 6C). Additional co-IP analyses showed that anti-p27 antibody failed to or could rarely pull down p62 protein in quiescent vSMCs, whereas HMGB1 stimulation significantly triggered the association of p27 with p62 in vSMCs (Figure 6D), suggesting that HMGB1 may promote p27 ubiquitination and its binding to p62. Subsequently, we sought to explore whether the proteasome or lysosome is involved in p27 protein degradation. Western blot analyses revealed that proteasomal inhibitor MG132 treatment failed to alter the HMGB1-induced decline in p27 protein levels in cultured vSMCs, thus excluding the influences of proteasome pathway on the degradation of p27 protein. Importantly, incubation with bafilomycin A1 further stabilized p27 protein level even in the presence of HMGB1 (Figure 6E). Similarly, genetic inhibition of autophagy induced by transfecting si*Atg5* drastically protected against HMGB1-induced downregulation of p27 protein (Figure 6F), suggesting that HMGB1 mediates p27 degradation in an autophagy flux-dependent manner.

We then explored the functional contribution of p27 to Sox9 expression, and found that genetic knockdown of *p27* in vSMCs led to an increase in Sox9 expression accompanied by a marked downregulation of vSMC marker genes at both the mRNA (Figure 6G) and protein levels (Figure 6H). However, *Sox9* knockdown markedly reversed these genes downregulation (Figure 6I), and attenuated *p27* knockdown-induced vSMC proliferation (Figure 6J) and migration (Figure 6K), confirming the involvement of p27 in Sox9 transcriptional expression and vSMC phenotypic modulation. Additionally, we cotransfected vSMCs with si*Atg5* and si*p27* followed by HMGB1 treatment, and found that *p27* knockdown significantly rescued Sox9 expression in vSMCs with autophagy inhibition (Figures 6L and 6M), demonstrating that autophagy promotes *Sox9* transcriptional expression by inducing p27 degradation.

p27 associates with p130/E2F4 complex on *Sox9* promoter

Previous reports have shown that p27 can inhibit targeted gene transcription by binding to gene promoter in association with the p130 and E2F4 (Jeannot et al., 2015; Pippa et al., 2012). We wondered whether p27 can alter *Sox9* transcriptional expression in vSMCs in this manner. We constructed pGL3-*Sox9* plasmid containing *Sox9* promoter sequences (−895 to −790) within the upstream of transcription start site, and cotransfected it with *p27*, *p130* and *E2F4* expressing plasmids in HEK293T cells. Chromatin immunoprecipitation (ChIP) identified the physical binding of p27, p130 and E2F4 to the *Sox9* promoter using indicated antibodies (Figure S7A). Luciferase reporter analyses showed that augmented *p27* in vSMCs realized by transfecting *p27* overexpressing plasmids was negatively associated with *Sox9* promoter activity (Figure 7A). In contrast, vSMCs with *p27* knocked down exhibited higher *Sox9* promoter activity than the control (Figure 7B). Furthermore, ChIP was performed using an anti-p27 antibody, and the results identified that endogenous p27 physically bound to the promoter region of *Sox9* in vSMCs (Figure 7C).

As shown in Figures S7B–S7E, HMGB1 treatment or autophagy inhibition failed to effect p130 and E2F4 expression in vSMCs. Notably, p27 was able to coimmunoprecipitate with endogenous p130 and E2F4 in vSMCs, as determined by co-IP (Figure 7D). We further performed ChIP assays using anti-p130 and

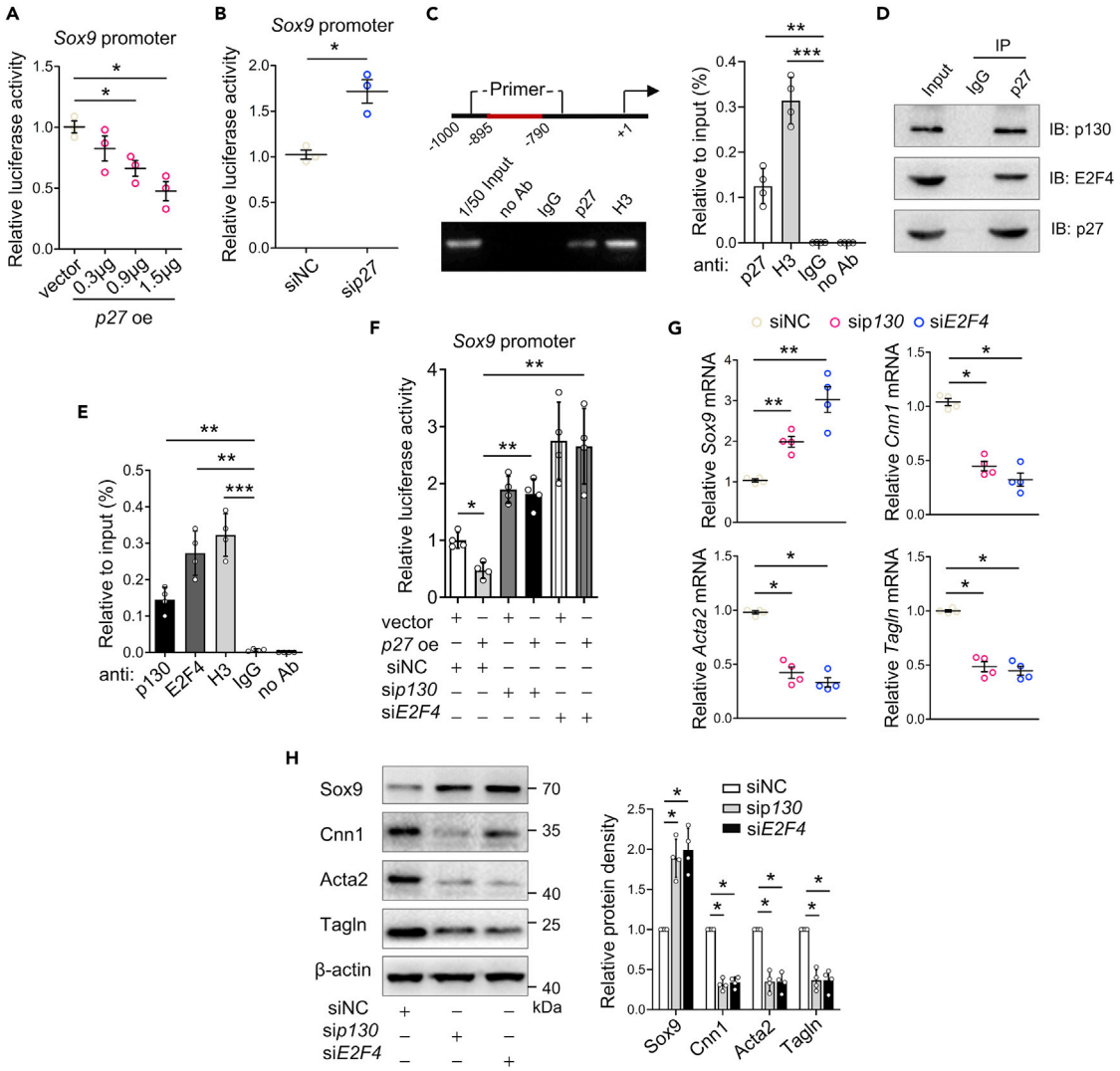

Figure 7. p27 associates with p130/E2F4 complex on *Sox9* promoters

(A) vSMCs were cotransfected with pGL3-*Sox9* reporter construct and *p27* overexpressing plasmid or empty vector for 48 h, *Sox9* promoter activity was measured by dual luciferase assays (means ± SEM *p < 0.05. n = 3).

(B) Dual luciferase assays were performed to evaluate *Sox9* promoter activity in vSMCs cotransfected with pGL3-*Sox9* reporter construct and si*p27* for 48 h (means ± SEM *p < 0.05. n = 3).

(C) Confirmation of the binding of p27 to *Sox9* promoter in vSMCs by ChIP assay followed by qRT-PCR and agarose gel electrophoresis. An anti-IgG antibody was used as the negative control, an anti-Histone H3 antibody was used as the positive control and no antibody was added as the empty control (means ± SEM **p < 0.01, ***p < 0.001. n = 4).

(D) Coimmunoprecipitation (co-IP) of p27 and p130/E2f4 complex in vSMCs (n = 4).

(E) ChIP of p130 and E2F4 protein in *Sox9* promoter in vSMCs (means ± SEM **p < 0.01, ***p < 0.001. n = 4).

(F) vSMCs were cotransfected with pGL3-*Sox9* reporter construct and *p27* overexpressing plasmid or *p130* siRNA or *E2F4* siRNA, *Sox9* promoter activity was measured by dual luciferase assays (means ± SEM *p < 0.05, **p < 0.01. n = 4).

(G and H) qRT-PCR and western blotting analyses of *Sox9*, *Cnn1*, *Acta2* and *Tagln* expression in vSMCs transfected with si*p130*, si*E2F4* or siNC for 48 h (means ± SEM *p < 0.05, **p < 0.01. n = 4).

anti-E2F4 antibodies, respectively, on extracts of vSMCs and found the binding of p130 and E2F4 to the *Sox9* promoter (Figure 7E). Moreover, knockdown of *p130* or *E2F4* markedly reversed *p27* overexpression-induced repression of *Sox9* promoter activity (Figure 7F), and further resulted in increased Sox9 expression and diminished expression of vSMC marker genes (Figures 7G and 7H), suggesting that p130/E2F4 repressive complex is essential for the recruitment of p27 to *Sox9* promoter, and together repress *Sox9* expression in vSMCs and maintain vSMC differentiation.

DISCUSSION

Phenotypic modulation of vSMCs has been functionally associated with the generation and progression of transplant arteriosclerosis (TA) (Boersema et al., 2012; Mitchell and Libby, 2007; Yu et al., 2018). Works presented in this study comprehensively unravel the expression and mechanism of Sox9 in vSMC phenotypic modulation *in vitro* and characterizes the influence of Sox9 on neointimal lesion formation in models of TA *in vivo*. We show that *Sox9* is transcriptionally upregulated in vSMCs in aortic allografts and HMGB1-treated vSMCs and is positively associated with vSMC phenotypic modulation, proliferation and migration. We also specifically identify a autophagy-mediated mechanism for *Sox9* transcriptional expression through controlling p27 protein degradation and restricting its binding to the p130/E2F4 complex located at the *Sox9* promoter. Of note, studies with rat graft arteriosclerosis models uncover functional repression of *Sox9* knockdown in the development of transplant arteriosclerotic lesions and highlights a potential TA intervention via the manipulation of Sox9.

The preliminary pathogenesis of TA features the activation of innate immunity, which is triggered at least in part by the release of endogenous damage-associated molecular patterns (DAMPs) by damaged or dying graft cells (Boersema et al., 2012; Todd and Palmer, 2017). DAMPs are characterized as a hidden immune system inside cells that predispose the recruitment of immune/inflammatory cells to injured grafts and the release of inflammatory mediators, which drives graft rejection and sterile inflammation after solid organ transplantation (Todd and Palmer, 2017). HMGB1, a nonhistone DNA-binding protein in nucleus, is one of the best-characterized DAMPs that can be actively expressed and secreted into the extracellular milieu by activated endothelial cells (ECs), vSMCs and inflammatory cells after organ transplantation (Todd and Palmer, 2017; Zou et al., 2021). Studies in mouse cardiac transplantation models have emphasized the importance of extracellular HMGB1 to the development and survival of chronic cardiac allografts, and specifically, increased HMGB1 is associated with the degree of graft vasculopathy because it triggers immune damage and graft inflammation (Zou et al., 2021). Moreover, blockage of HMGB1 markedly restrains vSMC migration and proliferation and protects against neointimal formation and vascular remodeling associated with the pathological progression of atherosclerosis (Chen et al., 2012). In this study, HMGB1 production was upregulated both in the plasma of rats undergoing allograft transplantation and aortic allografts within two weeks after transplantation, and HMGB1 stimulation promoted phenotypic modulation *in vitro* vSMCs, implying a functional contribution of HMGB1 to vSMC phenotypic modulation and graft arteriosclerosis triggered by alloimmune injury.

Transcription factor *Sox9* was initially reported to establish cell types during embryonic development (Jo et al., 2014), and also functions to maintain self-renewal and regeneration of adult tissues in homeostasis and injury (Furuyama et al., 2011). During the development of the circulatory system, repression of *Sox9* can drive the transdifferentiation of stem and progenitor cells toward the mature vSMC lineage characterized by the acquisition and maintenance of vSMC contractile properties, and facilitates the development of the embryonic vascular system (Briot et al., 2014). In adults, mature vSMCs display substantial phenotypical plasticity and retain the phenotype-modulation potential depending on the local microenvironment or genetic cues (Owens et al., 2004). Further supporting this notion, compelling studies have described the ability of vSMCs to transdifferentiate into chondrocytes in mouse injured carotids (Shen et al., 2011) and human calcified arteries (Tyson et al., 2003) characterized by the downregulation of vSMC contractile genes and increased *Sox9* expression. Mechanistically, *in vitro* evidence has demonstrated the functional contribution of Sox9 to vSMC phenotypic modulation by sequestering Myocd and subsequently repressing Srf activity (Xu et al., 2012). Support for this conclusion stems from the notion that in progenitors, Myocd or Srf alone is not sufficient to trigger complete vSMC differentiation (Owens et al., 2004; Yoshida et al., 2004). Combined with our previous studies showing that phenotypic modulation of medial vSMCs occurs in the early stage of allograft transplantation (Yu et al., 2018), the results of the present study uncover that forced Sox9 expression is positively associated with vSMC phenotypic modulation in aortic allografts 2 weeks after transplantation, and in cultured vSMCs exposed to HMGB1. In fact, vSMC phenotypic modulation precedes neointimal formation in aortic allografts (Bojakowski et al., 2000), and the migration and proliferation of dedifferentiated vSMCs into the endothelium are critical cellular events for neointimal formation following vascular injury (Owens et al., 2004). Evidence presented in our studies directly unravel, for the first time, that *Sox9* knockdown markedly blocks vSMC migration and proliferation and further ameliorates alloimmune injury-induced neointimal formation in aortic allografts, shedding light on a possible mechanism accounting for the beneficial contribution of Sox9 to TA after transplantation.

Our data discerns autophagy flux as an upstream regulator of Sox9 for mediating vSMC phenotypic modulation. Autophagy is a critical mediator implicated in cellular homeostasis and biological functions under stress conditions and diseases (Hale et al., 2013). Endogenous or exogenous HMGB1 is sufficient to activate autophagy by targeting RAGE (Huebener et al., 2014). Manipulating *RAGE* knockdown in aortic valve interstitial cells can restrict Sox9 upregulation induced by HMGB1 and alleviate aortic valve calcification (Wang et al., 2017). Moreover, it has been reported that genetic inhibition of autophagy is negatively associated with the protein expression of the liver progenitor marker Sox9 while promoting hepatic differentiation (Sugiyama et al., 2017). There is further evidence that autophagy activation induced by HMGB1 accounts for the upregulation of *Sox9* mRNA and protein *in vitro* vSMCs, highlighting that autophagy mediates *Sox9* expression at the transcriptional level. Recently, numerous studies have characterized the contribution of autophagy to vSMC phenotypic modulation in response to diverse pathological factors, such as PDGF, angiotensin II and oxLDL (Lu et al., 2021; Salabei et al., 2013). The present study shows that genetic knockdown and pharmacological inhibition of autophagy can repress vSMC phenotypic modulation induced by HMGB1, while this inhibition can be reversed by ectopic *Sox9*, implying a direct correlation between autophagy and *Sox9*-induced vSMC phenotypic modulation.

Another novel finding of our study is the identification of p27 as a mechanistic connection between autophagy and Sox9, which offers a better understanding of the possibility that cytoplasmic autophagy activation promotes *Sox9* transcription in the nucleus. p27, a cyclin-dependent kinase inhibitor, is highly expressed in the nucleus of quiescent cells (Hengst and Reed, 1996). Decreased *p27* expression seems important for vSMC proliferation, migration and neointimal hyperplasia in the pathogenesis of atherosclerosis and restenosis after vascular injury (Fan et al., 2019; Song et al., 2011). Recently, *Pippa* et al. reported another characterized function of p27 as a transcriptional repressor in the nucleus, where p27 associates with the promoter of its target genes together with the p130/E2F4 transcription repressor complex to exert transcriptional repressive activity (Pippa et al., 2012). The roles of the p130/E2F4 complex in DNA replication through the G1 phase have been extensively studied (Orlando et al., 2015). Associated with this complex, p27 binds to the SRR2 enhancer of *Sox2* that represses the transcription of *Sox2* in stem cells (Li et al., 2012a). For quiescent vSMCs, we also found that p27 can repress *Sox9* transcriptional activity by interacting with the p130/E2F4 complex located at the *Sox9* promoter, while the p27 protein was downregulated in HMGB1-stimulated vSMCs. In fact, upon mitogenic activation, p27 is translocated to the cytoplasm at G1 phase, which constitutes a major mechanism for its ubiquitin-mediated degradation via the ubiquitin ligase Kip1 ubiquitinylation-promoting complex (KPC) (Hengst and Reed, 1996; Kamura et al., 2004). The ubiquitin-proteasome has been recognized as a classical mechanism for p27 proteolytic degradation upon cell-cycle entry (Hengst and Reed, 1996). Moreover, an autophagy degradation pathway of p27 has also been extensively studied in an established genetic mouse model (Jia et al., 2015). In mammalian cells, endosomal protein sorting nexin 6 (SNX6) appears to interact with p27 in the lysosome, which facilitates p27 endolysosomal degradation upon mitogenic stimulation (Fuster et al., 2010). Further support for this mechanism comes from our present study showing that ubiquitinated p27 induced by HMGB1 physiologically binds to the autophagy adaptor protein p62/SQSTM1, whereas autophagy inactivation and lysosome inhibitor, but not a proteasome-specific inhibitor, restore the downregulation of p27 protein induced by HMGB in vSMCs, implying that activation of the autophagy-lysosomal pathway may be the underlying mechanism for p27 degradation in vSMCs exposed to HMGB1.

To date, autophagy triggered by most but not all cases in vSMCs, has a vasculoprotective effect and hastens the development of hyperproliferative and migratory phenotypes. In the present study, our results reveal that activated autophagic flux within vSMCs exposed to HMGB1 or alloimmune injury is essential for the acquisition of the dedifferentiated phenotype and proliferation and migration capacity. Moreover, activation of autophagy induced by PDGF, secreted protein sonic hedgehog or angiotensinII can enhance the tendency of vSMCs to proliferate and migrate (Li et al., 2012b; Lv et al., 2020; Salabei et al., 2013), facilitate the development of neointimal lesions and accelerate the progression of restenosis. Unlike these stimuli, TNF-α, IGF-1 and verapamil have been shown to promote autophagy activation in vSMCs but have opposite effects, mainly causing cell death (Jia et al., 2006; Salabei et al., 2012). This disparity regarding the role of autophagy in vSMC function and the outcome of diseased vasculature is possibly attributed to the stimulus context and stress intensity.

In summary, our study presents compelling evidence indicating that vSMC-specific *Sox9* knockdown is unfavorable to the maintenance of vSMC phenotypic modulation and delays the development of neointimal

formation after transplantation. Moreover, we show a novel autophagy-mediated mechanism for *Sox9* transcription in which the binding of p27 to the *Sox9* promoter, together with the p130/E2F4 complex is inhibited, suggesting that manipulating Sox9 may be an attractive therapeutic strategy for TA.

Limitations of the study

Circulating stem cells are reported to migrate into the intima and differentiate into neointimal cells, thereby contributing to neointimal formation (Sata et al., 2002). In fact, Sox9 is abundantly expressed in stem and progenitor cells and displays an inverse link to the transdifferentiation toward mature vSMCs (Briot et al., 2014). Although compelling evidence presented in this study have confirmed that selective *Sox9* knockdown in medial vSMCs in aortic allografts inhibits neointimal formation, the possibility of recruiting circulating stem cells into neointimal lesions regulated by Sox9 cannot be excluded, thus future studies are warranted to explore the role of Sox9 in modulating the recruitment and differentiation of stem cells after transplantation.

STAR★METHODS

Detailed methods are provided in the online version of this paper and include the following:

- KEY RESOURCES TABLE
- RESOURCE AVAILABILITY
  - Lead contact
  - Materials availability
  - Data and code availability
- EXPERIMENTAL MODEL AND SUBJECT DETAILS
  - Animals
  - Lentiviral vectors construction
  - Construction of aortic transplantation and tissue preparation
- METHOD DETAILS
  - Histology and morphometry
  - Immunostaining
  - RNA sequencing (RNA-seq) analysis
  - Cell culture, stimulation and transfection
  - Western blotting
  - Quantitative reverse transcription–polymerase chain reaction (qRT-PCR)
  - Cell counting Kit-8 and BrdU incorporation assay
  - Transwell assay
  - Luciferase activity assay
  - Chromatin immunoprecipitation (ChIP)
  - Transmission electron microscopy (TEM)
- QUANTIFICATION AND STATISTICAL ANALYSIS

SUPPLEMENTAL INFORMATION

Supplemental information can be found online at https://doi.org/10.1016/j.isci.2022.105161.

ACKNOWLEDGMENTS

This study was supported by the grants from National Natural Science Foundation of China to Z.S. (No. 81974040, 81670374), W.L. (No. 81974113), Q.H.Y. (No. 82000391), J.X.L. (No. 82101199) and by the grants from China Postdoctoral Science Foundation to Q.H.Y. (No. 2021M691142).

AUTHOR CONTRIBUTIONS

Q.H.Y.: Conceptualization, Data curation, Methodology, Validation, Visualization, Writing - original draft,-Funding acquisition. J.X.L.: Data curation, Methodology, Validation, Funding acquisition. X.C.Z.: Methodology, Validation, Visualization. X.K.Y.: Methodology, Visualization. P.Z.: Methodology, Formal analysis. C.Z.Y. Methodology, Visualization. W.L.: Conceptualization, Funding acquisition, Writing - review &editing. Z.F.S.: Conceptualization, Formal analysis, Funding acquisition, Writing - review &editing.

DECLARATION OF INTERESTS

The authors declare no competing interests.

Received: March 14, 2022
Revised: August 4, 2022
Accepted: September 15, 2022
Published: October 21, 2022

REFERENCES

Akiyama, H., Chaboissier, M.C., Martin, J.F., Schedl, A., and de Crombrugghe, B. (2002). The transcription factor Sox9 has essential roles in successive steps of the chondrocyte differentiation pathway and is required for expression of Sox5 and Sox6. Genes Dev. *16*, 2813–2828. https://doi.org/10.1101/gad.1017802.

Boersema, M., Katta, K., Rienstra, H., Molema, G., Nguyen, T.Q., Goldschmeding, R., Navis, G., van den Born, J., Popa, E.R., and Hillebrands, J.L. (2012). Local medial microenvironment directs phenotypic modulation of smooth muscle cells after experimental renal transplantation. Am. J. Transplant. *12*, 1429–1440. https://doi.org/10.1111/j.1600-6143.2012.04001.x.

Bojakowski, K., Religa, P., Bojakowska, M., Hedin, U., Gaciong, Z., and Thyberg, J. (2000). Arteriosclerosis in rat aortic allografts: early changes in endothelial integrity and smooth muscle phenotype. Transplantation *70*, 65–72.

Briot, A., Jaroszewicz, A., Warren, C.M., Lu, J., Touma, M., Rudat, C., Hofmann, J.J., Airik, R., Weinmaster, G., Lyons, K., et al. (2014). Repression of Sox9 by Jag1 is continuously required to suppress the default chondrogenic fate of vascular smooth muscle cells. Dev. Cell *31*, 707–721. https://doi.org/10.1016/j.devcel.2014.11.023.

Chen, J., Zhang, J., Xu, L., Xu, C., Chen, S., Yang, J., and Jiang, H. (2012). Inhibition of neointimal hyperplasia in the rat carotid artery injury model by a HMGB1 inhibitor. Atherosclerosis *224*, 332–339. https://doi.org/10.1016/j.atherosclerosis.2012.07.020.

Chih, S., Chong, A.Y., Mielniczuk, L.M., Bhatt, D.L., and Beanlands, R.S.B. (2016). Allograft vasculopathy: the Achilles' heel of heart transplantation. J. Am. Coll. Cardiol. *68*, 80–91. https://doi.org/10.1016/j.jacc.2016.04.033.

Fan, Y., Chen, Y., Zhang, J., Yang, F., Hu, Y., Zhang, L., Zeng, C., and Xu, Q. (2019). Protective role of RNA helicase DEAD-box protein 5 in smooth muscle cell proliferation and vascular remodeling. Circ. Res. *124*, e84–e100. https://doi.org/10.1161/CIRCRESAHA.119.314062.

Furuyama, K., Kawaguchi, Y., Akiyama, H., Horiguchi, M., Kodama, S., Kuhara, T., Hosokawa, S., Elbahrawy, A., Soeda, T., Koizumi, M., et al. (2011). Continuous cell supply from a Sox9-expressing progenitor zone in adult liver, exocrine pancreas and intestine. Nat. Genet. *43*, 34–41. https://doi.org/10.1038/ng.722.

Fuster, J.J., González, J.M., Edo, M.D., Viana, R., Boya, P., Cervera, J., Verges, M., Rivera, J., and Andrés, V. (2010). Tumor suppressor p27(Kip1) undergoes endolysosomal degradation through its interaction with sorting nexin 6. FASEB J *24*, 2998–3009. https://doi.org/10.1096/fj.09-138255.

Geisterfer, A.A., Peach, M.J., and Owens, G.K. (1988). Angiotensin II induces hypertrophy, not hyperplasia, of cultured rat aortic smooth muscle cells. Circ. Res. *62*, 749–756. https://doi.org/10.1161/01.res.62.4.749.

Gordon, C.T., Tan, T.Y., Benko, S., Fitzpatrick, D., Lyonnet, S., and Farlie, P.G. (2009). Long-range regulation at the SOX9 locus in development and disease. J. Med. Genet. *46*, 649–656. https://doi.org/10.1136/jmg.2009.068361.

Hale, A.N., Ledbetter, D.J., Gawriluk, T.R., and Rucker, E.B., 3rd (2013). Autophagy: regulation and role in development. Autophagy *9*, 951–972. https://doi.org/10.4161/auto.24273.

Hengst, L., and Reed, S.I. (1996). Translational control of p27Kip1 accumulation during the cell cycle. Science *271*, 1861–1864. https://doi.org/10.1126/science.271.5257.1861.

Hou, L., Srivastava, Y., and Jauch, R. (2017). Molecular basis for the genome engagement by Sox proteins. Semin. Cell Dev. Biol. *63*, 2–12. https://doi.org/10.1016/j.semcdb.2016.08.005.

Huebener, P., Gwak, G.Y., Pradere, J.P., Quinzii, C.M., Friedman, R., Lin, C.S., Trent, C.M., Mederacke, I., Zhao, E., Dapito, D.H., et al. (2014). High-mobility group box 1 is dispensable for autophagy, mitochondrial quality control, and organ function in vivo. Cell Metab. *19*, 539–547. https://doi.org/10.1016/j.cmet.2014.01.014.

Jeannot, P., Callot, C., Baer, R., Duquesnes, N., Guerra, C., Guillermet-Guibert, J., Bachs, O., and Besson, A. (2015). Loss of p27Kip(1) promotes metaplasia in the pancreas via the regulation of Sox9 expression. Oncotarget *6*, 35880–35892. https://doi.org/10.18632/oncotarget.5770.

Jia, G., Cheng, G., Gangahar, D.M., and Agrawal, D.K. (2006). Insulin-like growth factor-1 and TNF-alpha regulate autophagy through c-jun N-terminal kinase and Akt pathways in human atherosclerotic vascular smooth cells. Immunol. Cell Biol. *84*, 448–454. https://doi.org/10.1111/j.1440-1711.2006.01454.x.

Jia, W., He, M.X., McLeod, I.X., Guo, J., Ji, D., and He, Y.W. (2015). Autophagy regulates T lymphocyte proliferation through selective degradation of the cell-cycle inhibitor CDKN1B/p27Kip1. Autophagy *11*, 2335–2345. https://doi.org/10.1080/15548627.2015.1110666.

Jo, A., Denduluri, S., Zhang, B., Wang, Z., Yin, L., Yan, Z., Kang, R., Shi, L.L., Mok, J., Lee, M.J., and Haydon, R.C. (2014). The versatile functions of Sox9 in development, stem cells, and human diseases. Genes Dis. *1*, 149–161. https://doi.org/10.1016/j.gendis.2014.09.004.

Kamura, T., Hara, T., Matsumoto, M., Ishida, N., Okumura, F., Hatakeyama, S., Yoshida, M., Nakayama, K., and Nakayama, K.I. (2004). Cytoplasmic ubiquitin ligase KPC regulates proteolysis of p27(Kip1) at G1 phase. Nat. Cell Biol. *6*, 1229–1235. https://doi.org/10.1038/ncb1194.

Kumar, S., Liu, J., Pang, P., Krautzberger, A.M., Reginensi, A., Akiyama, H., Schedl, A., Humphreys, B.D., and McMahon, A.P. (2015). Sox9 activation highlights a cellular pathway of renal repair in the acutely injured mammalian kidney. Cell Rep. *12*, 1325–1338. https://doi.org/10.1016/j.celrep.2015.07.034.

Li, H., Collado, M., Villasante, A., Matheu, A., Lynch, C.J., Cañamero, M., Rizzoti, K., Carneiro, C., Martínez, G., Vidal, A., et al. (2012a). p27(Kip1) directly represses Sox2 during embryonic stem cell differentiation. Cell Stem Cell *11*, 845–852. https://doi.org/10.1016/j.stem.2012.09.014.

Li, H., Li, J., Li, Y., Singh, P., Cao, L., Xu, L.J., Li, D., Wang, Y., Xie, Z., Gui, Y., and Zheng, X.L. (2012b). Sonic hedgehog promotes autophagy of vascular smooth muscle cells. Am. J. Physiol. Heart Circ. Physiol. *303*, H1319–H1331. https://doi.org/10.1152/ajpheart.00160.2012.

Lodhi, S.A., Lamb, K.E., and Meier-Kriesche, H.U. (2011). Solid organ allograft survival improvement in the United States: the long-term does not mirror the dramatic short-term success. Am. J. Transplant. *11*, 1226–1235. https://doi.org/10.1111/j.1600-6143.2011.03539.x.

Lu, W., Zhou, Y., Zeng, S., Zhong, L., Zhou, S., Song, H., Ding, R., Zhong, G., Li, Q., Hu, Y., et al. (2021). Loss of FoxO3a prevents aortic aneurysm formation through maintenance of VSMC homeostasis. Cell Death Dis. *12*, 378. https://doi.org/10.1038/s41419-021-03659-y.

Luanpitpong, S., Li, J., Manke, A., Brundage, K., Ellis, E., McLaughlin, S.L., Angsutararux, P., Chanthra, N., Voronkova, M., Chen, Y.C., et al. (2016). SLUG is required for SOX9 stabilization and functions to promote cancer stem cells and metastasis in human lung carcinoma. Oncogene *35*, 2824–2833. https://doi.org/10.1038/onc.2015.351.

Lv, X.F., Zhang, Y.J., Liu, X., Zheng, H.Q., Liu, C.Z., Zeng, X.L., Li, X.Y., Lin, X.C., Lin, C.X., Ma, M.M., et al. (2020). TMEM16A ameliorates vascular remodeling by suppressing autophagy via inhibiting Bcl-2-p62 complex formation. Theranostics *10*, 3980–3993. https://doi.org/10.7150/thno.41028.

Mitchell, R.N., and Libby, P. (2007). Vascular remodeling in transplant vasculopathy. Circ. Res. *100*, 967–978. https://doi.org/10.1161/01.RES.0000261982.76892.09.

Naik, V., Leaf, E.M., Hu, J.H., Yang, H.Y., Nguyen, N.B., Giachelli, C.M., and Speer, M.Y. (2012). Sources of cells that contribute to atherosclerotic intimal calcification: an in vivo genetic fate mapping study. Cardiovasc. Res. *94*, 545–554. https://doi.org/10.1093/cvr/cvs126.

Orlando, S., Gallastegui, E., Besson, A., Abril, G., Aligué, R., Pujol, M.J., and Bachs, O. (2015). p27Kip1 and p21Cip1 collaborate in the regulation of transcription by recruiting cyclin-Cdk complexes on the promoters of target genes. Nucleic Acids Res. *43*, 6860–6873. https://doi.org/10.1093/nar/gkv593.

Orriols, M., Varona, S., Martí-Pàmies, I., Galán, M., Guadall, A., Escudero, J.R., Martín-Ventura, J.L., Camacho, M., Vila, L., Martínez-González, J., and Rodríguez, C. (2016). Down-regulation of Fibulin-5 is associated with aortic dilation: role of inflammation and epigenetics. Cardiovasc. Res. *110*, 431–442. https://doi.org/10.1093/cvr/cvw082.

Owens, G.K., Kumar, M.S., and Wamhoff, B.R. (2004). Molecular regulation of vascular smooth muscle cell differentiation in development and disease. Physiol. Rev. *84*, 767–801. https://doi.org/10.1152/physrev.00041.2003.

Pippa, R., Espinosa, L., Gundem, G., García-Escudero, R., Dominguez, A., Orlando, S., Gallastegui, E., Saiz, C., Besson, A., Pujol, M.J., et al. (2012). p27Kip1 represses transcription by direct interaction with p130/E2F4 at the promoters of target genes. Oncogene *31*, 4207–4220. https://doi.org/10.1038/onc.2011.582.

Rogov, V., Dötsch, V., Johansen, T., and Kirkin, V. (2014). Interactions between autophagy receptors and ubiquitin-like proteins form the molecular basis for selective autophagy. Mol. Cell *53*, 167–178. https://doi.org/10.1016/j.molcel.2013.12.014.

Salabei, J.K., Balakumaran, A., Frey, J.C., Boor, P.J., Treinen-Moslen, M., and Conklin, D.J. (2012). Verapamil stereoisomers induce antiproliferative effects in vascular smooth muscle cells via autophagy. Toxicol. Appl. Pharmacol. *262*, 265–272. https://doi.org/10.1016/j.taap.2012.04.036.

Salabei, J.K., Cummins, T.D., Singh, M., Jones, S.P., Bhatnagar, A., and Hill, B.G. (2013). PDGF-mediated autophagy regulates vascular smooth muscle cell phenotype and resistance to oxidative stress. Biochem. J. *451*, 375–388. https://doi.org/10.1042/BJ20121344.

Sata, M., Saiura, A., Kunisato, A., Tojo, A., Okada, S., Tokuhisa, T., Hirai, H., Makuuchi, M., Hirata, Y., and Nagai, R. (2002). Hematopoietic stem cells differentiate into vascular cells that participate in the pathogenesis of atherosclerosis. Nat. Med. *8*, 403–409. https://doi.org/10.1038/nm0402-403.

Schepers, G.E., Teasdale, R.D., and Koopman, P. (2002). Twenty pairs of sox: extent, homology, and nomenclature of the mouse and human sox transcription factor gene families. Dev. Cell *3*, 167–170. https://doi.org/10.1016/s1534-5807(02)00223-x.

Shen, J., Yang, M., Jiang, H., Ju, D., Zheng, J.P., Xu, Z., Liao, T.D., and Li, L. (2011). Arterial injury promotes medial chondrogenesis in Sm22 knockout mice. Cardiovasc. Res. *90*, 28–37. https://doi.org/10.1093/cvr/cvq378.

Song, P., Wang, S., He, C., Wang, S., Liang, B., Viollet, B., and Zou, M.H. (2011). AMPKα2 deletion exacerbates neointima formation by upregulating Skp2 in vascular smooth muscle cells. Circ. Res. *109*, 1230–1239. https://doi.org/10.1161/CIRCRESAHA.111.250423.

Sugiyama, M., Yoshizumi, T., Yoshida, Y., Bekki, Y., Matsumoto, Y., Yoshiya, S., Toshima, T., Ikegami, T., Itoh, S., Harimoto, N., et al. (2017). p62 promotes amino acid sensitivity of mTOR pathway and hepatic differentiation in adult liver stem/progenitor cells. J. Cell. Physiol. *232*, 2112–2124. https://doi.org/10.1002/jcp.25653.

Todd, J.L., and Palmer, S.M. (2017). Danger signals in regulating the immune response to solid organ transplantation. J. Clin. Invest. *127*, 2464–2472. https://doi.org/10.1172/JCI90594.

Tyson, K.L., Reynolds, J.L., McNair, R., Zhang, Q., Weissberg, P.L., and Shanahan, C.M. (2003). Osteo/chondrocytic transcription factors and their target genes exhibit distinct patterns of expression in human arterial calcification. Arterioscler. Thromb. Vasc. Biol. *23*, 489–494. https://doi.org/10.1161/01.ATV.0000059406.92165.31.

Wang, B., Cai, Z., Liu, B., Liu, Z., Zhou, X., Dong, N., and Li, F. (2017). RAGE deficiency alleviates aortic valve calcification in ApoE(-/-) mice via the inhibition of endoplasmic reticulum stress. Biochim. Biophys. Acta Mol. Basis Dis. *1863*, 781–792. https://doi.org/10.1016/j.bbadis.2016.12.012.

Xu, Z., Ji, G., Shen, J., Wang, X., Zhou, J., and Li, L. (2012). SOX9 and myocardin counteract each other in regulating vascular smooth muscle cell differentiation. Biochem. Biophys. Res. Commun. *422*, 285–290. https://doi.org/10.1016/j.bbrc.2012.04.149.

Yoshida, T., Kawai-Kowase, K., and Owens, G.K. (2004). Forced expression of myocardin is not sufficient for induction of smooth muscle differentiation in multipotential embryonic cells. Arterioscler. Thromb. Vasc. Biol. *24*, 1596–1601. https://doi.org/10.1161/01.ATV.0000137190.63214.c5.

Yu, Q., Li, W., Jin, R., Yu, S., Xie, D., Zheng, X., Zhong, W., Cheng, X., Hu, S., Li, M., et al. (2019). PI3Kγ (phosphoinositide 3-kinase γ) regulates vascular smooth muscle cell phenotypic modulation and neointimal formation through CREB (cyclic AMP-response element binding protein)/YAP (Yes-Associated protein) signaling. Arterioscler. Thromb. Vasc. Biol. *39*, e91–e105. https://doi.org/10.1161/ATVBAHA.118.312212.

Yu, Q., Li, W., Xie, D., Zheng, X., Huang, T., Xue, P., Guo, B., Gao, Y., Zhang, C., Sun, P., et al. (2018). PI3Kγ promotes vascular smooth muscle cell phenotypic modulation and transplant arteriosclerosis via a SOX9-dependent mechanism. EBioMedicine *36*, 39–53. https://doi.org/10.1016/j.ebiom.2018.09.013.

Zhao, B., Yoganathan, K., Li, L., Lee, J.Y., Zúñiga-Pflücker, J.C., and Love, P.E. (2019). Notch and the pre-TCR coordinate thymocyte proliferation by induction of the SCF subunits Fbxl1 and Fbxl12. Nat. Immunol. *20*, 1381–1392. https://doi.org/10.1038/s41590-019-0469-z.

Zou, H., Ming, B., Li, J., Xiao, Y., Lai, L., Gao, M., Xu, Y., Tan, Z., Gong, F., and Zheng, F. (2021). Extracellular HMGB1 contributes to the chronic cardiac allograft vasculopathy/fibrosis by modulating TGF-beta1 signaling. Front. Immunol. *12*, 641973. https://doi.org/10.3389/fimmu.2021.641973.

STAR★METHODS

KEY RESOURCES TABLE

REAGENT or RESOURCE	SOURCE	IDENTIFIER
Antibodies		
Mouse anti-Myocardin antibody	Santa Cruz Biotechnology	Cat#sc-21559; RRID: AB_2251111
Rabbit anti-p27^{Kip1} antibody	Santa Cruz Biotechnology	Cat#sc-528; RRID: AB_632129
Rabbit anti-Sox9 antibody	Abcam	Cat#ab185230; RRID: AB_2715497
Rabbit anti-Tagln antibody	Abcam	Cat#ab14106; RRID: AB_443021
Mouse anti-Acta2 antibody	Abcam	Cat#ab7817; RRID: AB_262054
Rabbit anti-Calponin1 antibody	Abcam	Cat#ab46794; RRID: AB_2291941
Rabbit anti-Hmgb1 antibody	Abcam	Cat#ab79823; RRID: AB_1603373
Rabbit anti-SQSTM1/p62 antibody	Abcam	Cat#ab109012; RRID: AB_2810880
Rabbit anti-Histone H3 antibody	Abcam	Cat#ab1791; RRID: AB_302613
Rabbit anti-Atg5 antibody	Cell Signaling Technology	Cat#12994; RRID: AB_2630393
Rabbit anti-LC3I/II antibody	Cell Signaling Technology	Cat#12741; RRID: AB_2617131
Rabbit anti-p27^{Kip1} antibody	Cell Signaling Technology	Cat#3686; RRID: AB_2077850
Rabbit anti-Srf antibody	Cell Signaling Technology	Cat#5147; RRID: AB_10694554
Rabbit anti-E2F4 antibody	Cell Signaling Technology	Cat#40291; RRID: AB_2799174
Mouse anti-Ubiquitin antibody	Cell Signaling Technology	Cat#3936; RRID: AB_331292
Rabbit anti-Rbl2 antibody	Cell Signaling Technology	Cat#13610; RRID: AB_2798274
Rabbit anti-PCNA antibody	Cell Signaling Technology	Cat#13110; RRID: AB_2636979
Mouse anti-Myc-tag antibody	Cell Signaling Technology	Cat#2276; RRID: AB_331783
Rabbit anti-HA-tag antibody	Cell Signaling Technology	Cat#3724; RRID: AB_1549585
Rabbit anti-Flag-Tag antibody	Cell Signaling Technology	Cat#14793; RRID: AB_2572291
Rabbit anti-IgG antibody	Cell Signaling Technology	Cat#3900; RRID: AB_1550038
Mouse anti-IgG antibody	Sigma-Aldrich	Cat#I5381; RRID: AB_1163670
Rabbit anti-Histone H3 antibody	Boster Biological Technology	Cat#BM4715
Rabbit anti-β-actin antibody	Boster Biological Technology	Cat#BA2305
Chemicals, peptides, and recombinant proteins		
Recombinant HMGB1	BioLegend	Cat#557804
Bafilomycin A1	Sigma-Aldrich	Cat#19-148
MG132	Sigma-Aldrich	Cat#M8699
Lipofectamine 3000	Invitrogen	Cat#P/N100022050
Polybrene	Sigma-Aldrich	Cat#TR-1003-G
Puromycin	Absin	Cat#abs42025969
Critical commercial assays		
Cell Counting Kit-8 (CCK-8)	Dojindo	CK04
BrdU Labeling and Detection kit	Biovision	K306-200
PrimeScript RT Master Mix kit	Takara	RR036A-1
SYBR Premix Ex Taq kit	Takara	RR420A
SimpleCHIP ® Plus Sonication Chromatin IP kit	Cell Signaling Technology	56,383
Dual-luciferase reporter kit	Promega	E2920
HMGB1 ELISA kit	Uscn Life Science	SEA399Hu

(*Continued on next page*)

Continued

REAGENT or RESOURCE	SOURCE	IDENTIFIER
Deposited data		
Raw and analyzed data of RNA-seq	This paper	BioProject accession: PRJNA761586
Raw and analyzed data of RNA-seq	This paper	BioProject accession: PRJNA866874
Experimental models: Cell lines		
HEK293T cell line	ATCC	Cat# CRL_3216, RRID:CVCL_0063
Oligonucleotides		
siAtg5 targeting sequence: 5′-GUAGGUGAUCAACGAAAUTT-3′	GenePharma	N/A
sip27 targeting sequence: 5′-GGCCAACAGAACAGAAGAATT-3′	GenePharma	N/A
siE2F4 targeting sequence: 5′-GCACTGAAGTCTCAGATGT-3′	RiBo biotechnology	N/A
siRbl2 targeting sequence: 5′-GAACAGATACTCAGGTCAT-3′	RiBo biotechnology	N/A
siSox9 targeting sequence: 5′-CGGCCGCGACTCT AGAATTCTGTTTGAATGAGGCTTCAGTAC-3′	GeneChem	N/A
Primers for *Sox9*, see Table S1	Sangon Biotech	N/A
Primers for *Myocardin*, see Table S1	Sangon Biotech	N/A
Primers for *Srf*, see Table S1	Sangon Biotech	N/A
Primers for *Tagln*, see Table S1	Sangon Biotech	N/A
Primers for *Calponin1*, see Table S1	Sangon Biotech	N/A
Primers for *Acta2*, see Table S1	Sangon Biotech	N/A
Primers for *Atg5*, see Table S1	Sangon Biotech	N/A
Primers for *p27*, see Table S1	Sangon Biotech	N/A
Primers for *E2F4*, see Table S1	Sangon Biotech	N/A
Primers for *Rbl2*, see Table S1	Sangon Biotech	N/A
Primers for *Hmgb1*, see Table S1	Sangon Biotech	N/A
Primers for *Gapdh*, see Table S1	Sangon Biotech	N/A
Primers for *Sox9* for CHIP, see Table S1	Sangon Biotech	N/A
Recombinant DNA		
pcDNA3.1-*Sox9*	GeneChem	N/A
pcDNA3.1-*p27*	GeneChem	N/A
pcDNA3.1-Flag-tagged *Myocardin*	GeneChem	N/A
pGL3-*Sox9* promoter-luci. plasmid	GeneChem	N/A
pcDNA3.1-*p130*	GeneChem	N/A
pcDNA3.1-*E2F4*	GeneChem	N/A
Software and algorithms		
GraphPad Prism 9 software	GraphPad Software Inc.	RRID:SCR_002798
ImageJ software	NIH	RRID:SCR_003070
Image-Pro Plus software	Media Cybernetics, Inc.	RRID:SCR_016879
ChemiDoc imaging system	Bio-Rad	RRID:SCR_019684
Adobe Photoshop	Adobe	RRID:SCR_014199

RESOURCE AVAILABILITY

Lead contact

Further information and requests for resources and reagents should be directed to and will be fulfilled by the lead contact, Zifang Song (zsong@hust.edu.cn).

Materials availability

This study did not generate new unique reagents.

Data and code availability

- RNA-seq data have been deposited at NCBI database and are publicly available as of the date of publication. Accession numbers are listed in the key resources table.
- This paper does not report original code.
- Any additional information required to reanalyze the data reported in this paper is available from the lead contact upon request.

EXPERIMENTAL MODEL AND SUBJECT DETAILS

Animals

Male Brown Norway (BN, 4-5 weeks old) rats and Lewis (4-5 weeks old) rats were purchased from HFK Bioscience Co. (Beijing, China) and housed under specific pathogen-free conditions. All animal procedures were conducted according to the guidelines of National Institutes of Health (NIH) for the Care and Use of Laboratory Animals and the guidelines of Animal Research: Reporting of *In Vivo* Experiments (ARRIVE), and were approved by the ethics committee of Tongji Medical College, Huazhong University of Science and Technology (Wuhan, China).

Lentiviral vectors construction

Recombinant lentiviral vectors carrying rat *Sox9*-targeting shRNA together with a specific *Tagln* promoter (sh*Sox9*) (GeneChem, Shanghai, China) or its corresponding negative control (shNC) were designed and generated (Yu et al., 2018). Briefly, a specific mouse *Tagln* promoter (−441 to +41, GenBank accession no. U36589) and selective rat *Sox9* (GenBank accession no. NM_08043) shRNA sequence were cloned into the EcoRI/EcoRI restriction sites of CV026 vectors, respectively. The 5–3′ sequence for *Sox9* shRNA is: sense, CGGCCGCGACTCTAGAATTCTGTTTGAATGAGGCTTCAGTAC. The recombinant lentiviral vectors were cotransfected with packaging plasmids pHelper 1.0 and pHelper 2.0 into 293 T cells using Lipofectamine 2000. After 48 h, packaged lentivirus in the supernatant were collected and purified using ultracentrifugation. Affinity chromatography was performed to measure the concentration and purity of lentiviral particles. The functional viral titers were analyzed by real-time PCR.

Construction of aortic transplantation and tissue preparation

Rat model of abdominal aortic transplantation was established using a modified technique. Male Lewis rats were used as donors, syngeneic recipients and allogeneic recipients. Male BN rats served as donors. After anesthesia with an inhaled anesthesia mixture of isoflurane (3%) and oxygen (1 L/min), a segment of abdominal aorta approximately 1 cm in length was isolated from the donors and gently perfused 3-5 times with pre-cooling DMEM. The clean aortic grafts were soaked into opti-MEM medium containing lentiviruses expressing *Sox9*-targeting shRNA (sh*Sox9*) with a specific *Tagln* promoter (GeneChem, Shanghai, China) or the corresponding negative control (shNC) (2×10^7 TU/ml) in the presence of polybrene (5 μg/mL) for 30 min under ice bath. Subsequently, the aortic graft was transplanted orthotopically into the position below the renal artery and above the iliac bifurcation. A proximal end-to-end microsurgical anastomosis was performed with 11–0 single interrupted nylon suture. The ischemic time was approximately 1 h. Metamizole (50 mg/100 mL in drinking water) was used for painkilling for 3 days after transplantation.

The recipient rats were euthanized with an overdose of pentobarbital sodium (180 mg/kg) 2 and 8 weeks after transplantation. For transcriptome microarray and PCR analyses at 2 weeks, after *in situ* cardiac perfusion with ice-cold sterile saline, the adventitial loose connective tissue of aortic grafts was bluntly stripped from the surface of the artery by pulling the adventitia off the artery with two pairs of sterile forceps, and the endangium of aortic grafts was carefully removed by advancing an angioplasty guide wire into aortic lumen and pulling back 2-3 times. The naked media was visible and medial vSMCs in aortic grafts were collected. Aortic grafts with adventitia removal at 8 weeks were also collected for PCR analysis. For histological and immunostaining analyses, rats were situ perfused with ice-cold sterile saline followed by perfusion fixation with 4% paraformaldehyde, aortic grafts were then harvested and fixed with 4% paraformaldehyde overnight at room temperature.

METHOD DETAILS

Histology and morphometry

The arterial segments were subjected to dehydration in ethanol and xylene, and embedded in paraffin. The aortic grafts were trimmed at least 2 mm from the suture line and divided into two parts from the center. Serial cross-sections (5-μm thick) were cut proximal to the middle of the graft to avoid the suture line. 5 cross-sections (250 μm intervals) from each graft were selected and stained with hematoxylin-eosin (H&E) and elastic tissue fibers-Verhoeff's Van Gieson (EVG). Morphometry analyses of digital images of stained sections were carried out by two independent investigators blinded to the experimental design using Image-Pro Plus software (Media Cybernetics, Inc. Silver Spring, MD, USA). The lumen area, intimal area, medial area, and total vessel area were measured at each level (Yu et al., 2019). The mean neointimal area, intima/media ratio, and lumen stenosis ratio was calculated.

Immunostaining

Immunohistochemistry was performed on paraffin-embedded sections using the avidin-biotin-peroxidase complex method. Undergoing deparaffinize, rehydration, antigen retrieval and blocking, tissue sections were incubated with primary antibodies against Hmgb1 (1 μg/mL), PCNA (0.2 μg/mL) and Sox9 (0.5 μg/mL). Isotype-matched IgG antibodies were used as negative controls. Subsequently, the sections were incubated with biotinylated secondary antibodies and visualized by 3,3′-diaminobenzidine (DAB), followed by nuclear counterstaining with hematoxylin by using a histostain-plus kit (Boster Biotechnology, Wuhan, China) according to the manufacturer's instructions. Images were taken under microscope, and the positive staining area or cell number in tissue sections were analyzed by Image-Pro Plus software (Media Cybernetics, Inc. Silver Spring, MD, USA). The results were presented as percentage of the total medial area or cells.

Immunofluorescence staining was performed on paraffin-embedded sections and cultured vSMCs using the following antibodies: Cnn1 (2 μg/mL), Acta2 (1:200), Tagln (2 μg/mL), Sox9 (2 μg/mL) and LC3I/II (2 μg/mL). Immunoreactions were visualized using FITC or CY3-conjugated secondary antibodies (1:200). Nuclei were counterstained with with hoechst (Invitrogen). Images were taken under fluorescence microscope and the positive staining area or cell number in tissue sections were analyzed by Image-Pro Plus software (Media Cybernetics, Inc. Silver Spring, MD, USA). The results were presented as percentage of the total traced area or cells.

RNA sequencing (RNA-seq) analysis

Total RNA was extracted from the medial vSMCs in aortic grafts using TRIzol Reagent (Invitrogen) following the manufacturer's instructions. RNA quality was assessed with 2100 Bioanalyser (Agilent) and quantified by the ND-2000 (NanoDrop Technologies). 1 μg of total RNA was used for RNA-seq transcriptome library preparation with a TruSeq™ RNA sample preparation Kit (Illumina, SanDiego, CA). After quantified by TBS380 (Picogreen), RNA libraries were deep sequenced with HiSeq xten/NovaSeq 6000 sequencer (Illumina, San Diego, CA) at an average of 30 million reads per samples (2 × 150bp read length). The raw paired end reads were trimmed and quality controlled by SeqPrep (https://github.com/jstjohn/SeqPrep) and Sickle (https://github.com/najoshi/sickle) with default parameters. Then clean reads were separately aligned to reference genome with orientation mode using HISAT2 system (http://ccb.jhu.edu/software/hisat2/index.shtml). Read count and expression of each transcript was calculated according to the transcripts per million reads (TPM) method. RNA-Seq by Expectation Maximization (RSEM) (http://deweylab.biostat.wisc.edu/rsem/) was used to quantify gene abundances, taking paired-end reads, length of reads, etc. into account. Differential genes expression between two groups were assessed using DESeq2 with adjusted p value < 0.05 and $|\log2 \text{(fold change)}| \geq 1$ were considered to be significantly different expressed genes. Principal component analysis (PCA) was performed to analyze sample clustering. Gene ontology (GO) functional enrichment and Kyoto Encyclopedia of Genes and Genomes (KEGG) enrichment analysis were done by Goatools and KOBAS. Differential expression genes were significantly enriched in GO terms with Bonferroni-corrected p value < 0.05 compared with the whole-transcriptome background. All raw data have been uploaded to the Sequence Read Archive (SRA, NCBI) database with the BioProject accession number PRJNA761586 (Release date: 2025-09-07) and PRJNA866874 (Release date: 2026-08-06).

Cell culture, stimulation and transfection

Primary vSMCs were isolated from thoracic aorta of BN rats according to an enzymatic digestion protocol described by Geisterfer AA et al. (Geisterfer et al., 1988). All *in vitro* experiments were performed on cells passaged for 3 to 6 generations. Before reagents treatment, vSMCs were cultured in medium deprived of serum for 24 h to achieve quiescence.

For intervention experiments, quiescent cells were pretreated with 200 nM Bafilomycin A1 (Sigma, USA) or 10 μM MG132 (Sigma, USA) for 60 min prior to 100 ng/mL recombinant HMGB1 (BioLegend, USA) stimulation.

For *Sox9* knockdown, vSMCs were transfected with recombinant lentiviruses carring short hairpin RNA targeting *Sox9* (sh*Sox9*) driven by a specific *Tagln* promoter (GeneChem, Shanghai, China) and its corresponding negative control shRNA (shNC) according to the manufacturer's protocol at a MOI of 100 in medium containing 5 μg/mL polybrene (Sigma, USA). Transfected cells were selected by 3 ug/ml puromycin (Absin, China) for 72 h.

Knockdown of *Atg5*, *p27*, *p130* and *E2F4*, respectively, were realized by siRNA transfection according to the manufacturer's protocol. In some experiments, vSMCs transfected with si*Atg5*, si*p27*, si*p130* and si*E2F4* were further stimulated with 100 ng/mL HMGB1 at indicated time points and harvested for cell experiments.

For plasmid transfection, cultured vSMCs were transfected with plasmid pcDNA3.1 encoding rat *Sox9* gene and *p27* gene and its control plasmid pcDNA3.1(vector), and HEK293T cell line (ATCC, Cat# CRL_3216, RRID: CVCL_0063) were transfected with plasmid pcDNA3.1 encoding rat Flag-tagged *Myocardin* by using transfection reagent Lipofectamine 3000 (Invitrogen, USA) according to the manufacturer's protocol. Total RNA and protein were extracted 48 h after transfection.

Western blotting

Cells were lysed, total protein or nuclear protein fractions were extracted by using protein extraction kit according to the manufacturer's protocol (Boster Biological Technology, Wuhan, China). Immunoreactivity was visualized using corresponding antibodies and recorded using ChemiDoc imaging system (Bio-Rad). Relative protein expression was normalized to β-actin.

Quantitative reverse transcription–polymerase chain reaction (qRT-PCR)

Quantitative RT-PCR was performed with specific primers (see Table S1 in the Supplementary materials). Briefly, total RNA was extracted from rat aortic grafts and cultured vSMCs using TRIzol Reagent. 1 μg of total RNA was reverse-transcribed into cDNA using PrimeScript RT Master Mix and then subjected to quantitative PCR analysis using the SYBR Premix Ex Taq kit with specific primers. Relative RNA expression was quantified by normalizing to housekeeping gene Gapdh, and the value was calculated by using the 2(-Delta Delta CT) method.

Cell counting Kit-8 and BrdU incorporation assay

Cell proliferation was evaluated by Cell Counting Kit-8 (CCK-8) assay and BrdU incorporation assay. vSMCs transfected with sh*Sox9* or si*Atg5* were treated or without 100 mg/mL HMGB1 (BioLegend, USA) for indicated time. Afterward, the cells were incubated with CCK-8 solution (Dojindo, Kumamoto, Japan) or BrdU-labeling solution (Biovision, California, USA), and the absorbance at 450nm was detected using a microplate reader.

Transwell assay

Transwell assay was applied to evaluate cell migration. vSMCs transfected with sh*Sox9*, si*Atg5* or its corresponding control were incubated with HMGB1 for 48 h. After digestion, 1×10^5 cells in 100ul of FBS-free DMEM were seeded onto the upper chambers with a filter membrane (8-μm pore size) of 24-well plates. 2% FBS in free DMEM acted as a dynamic factor was added to the lower chambers. After incubation for further 6 h at 37°C, migrated cells on the lower surface of the filters were fixed and stained with 0.1% crystal violet solution and imaged under bright-field microscope. Migration rate was indicated by the cellular number quantified in five different fields.

Luciferase activity assay

Cultured vSMCs were cotransfected with dual luciferase reporter constructs containing *Sox9* promoter sequence (1 kb upstream with the transcription start site) and *p27* overexpressing plasmids, *p27* siRNA, *p130* siRNA or *E2F4* siRNA together with the renilla luciferase reporter plasmids containing thymidine kinase promoter using Lipofectamine 3000 transfection agent. Luciferase activities were detected using a dual-luciferase reporter assay kit (Promega, Madison, WI, USA) under the manufacturer's instruction. Firefly luciferase activity was normalized to Renilla activity.

Chromatin immunoprecipitation (ChIP)

ChIP was performed by utilizing SimpleCHIP Plus Sonication Chromatin IP kit according to the manufacturer's protocol. Briefly, vSMCs were cross-linked with 1% formaldehyde and sonicated to soluble chromatin with DNA fragments. Clean chromatin was incubated with indicated antibodies overnight at 4°C. Isotype-matched anti-IgG as the negative control. anti-Histone H3 as the positive control and no any antibodies as the empty control. The protein-DNA complex was precipitated by protein G magnetic beads, followed by a series of procedures including the elution of immunoprecipitates, the revision of protein-DNA cross-link and the purification of DNA. The DNA fragments were detected by PCR assays and agarose gel electrophoresis. The primer of *Sox9* used for PCR following ChIP is: 5′-GAAGGGAGGAGGGG TATTGC-3′ (forward) and 5′-GATCACTCGCGTCTTGCTC-3′ (reverse).

Transmission electron microscopy (TEM)

Cultured vSMCs and aortic grafts were fixed in 2.5% glutaraldehyde (Servicebio) and 1% osmic acid (Ted Pella Inc) followed by acetone dehydration. A Leica UC7 microtome (Leica) was used to prepared ultrathin sections, and these sections were stained with 2% alcoholic uranyl acetate and 2.6% lead citrate. Autophagic vacuoles were observed under a transmission electron microscope (Hitachi).

QUANTIFICATION AND STATISTICAL ANALYSIS

Statistical analyses were undertaken using GraphPad Prism version 5.0 (GraphPad Software Inc., San Diego, CA, USA) software. All values are presented as the means ± SEM Data distribution and equal variance analysis were determined using Shapiro-Wilk test and Levene test, respectively. When normal distribution was confirmed, unpaired two-tailed Student's *t* test was performed for statistical differences between two independent groups, or one-way ANOVA with Bonferroni post hoc test was conducted for multiple group comparisons. A p value <0.05 was considered statistically significant.